

## Low-Latitude Circulation and Mass Transport Pathways in a Model of the Tropical Atlantic Ocean\*

DAVID M. FRATANTONI

*Department of Physical Oceanography, Woods Hole Oceanographic Institution, Woods Hole, Massachusetts*

WILLIAM E. JOHNS

*Division of Meteorology and Physical Oceanography, Rosenstiel School of Marine and Atmospheric Science, University of Miami, Miami, Florida*

TAMARA L. TOWNSEND AND HARLEY E. HURLBURT

*Ocean Dynamics and Prediction Branch, Naval Research Laboratory, Stennis Space Center, Mississippi*

(Manuscript received 10 September 1998, in final form 15 September 1999)

### ABSTRACT

An eddy-resolving numerical ocean circulation model is used to investigate the pathways of low-latitude intergyre mass transport associated with the upper limb of the Atlantic meridional overturning cell (MOC). Numerical experiments with and without applied wind stress and an imposed MOC exhibit significant differences in intergyre transport, western boundary current intensity, and mesoscale ring production. The character of interaction between low-latitude wind- and overturning-driven circulation systems is found to be predominantly a linear superposition in the annual mean, even though nonlinearity in the form of diapycnal transport is essential to some segments of the mean pathway. Within a mesoscale band of 10–100 day period, significant nonlinear enhancement of near-surface variability is observed. In a realistically forced model experiment, a 14 Sv upper-ocean MOC return flow is partitioned among three pathways connecting the equatorial and tropical wind-driven gyres. A frictional western boundary current with both surface and intermediate depth components is the dominant pathway and accounts for 6.8 Sv of intergyre transport. A diapycnal pathway involving wind-forced equatorial upwelling and interior Ekman transport is responsible for 4.2 Sv. Translating North Brazil Current rings contribute approximately 3.0 Sv of intergyre transport.

### 1. Introduction

Cold, dense North Atlantic Deep Water (NADW) is convectively formed at high latitudes and exported southward across the equator into the Southern Ocean. The loss of NADW from the Atlantic basin is compensated by a northward replacement flow of warm thermocline and intermediate water. The resulting buoyancy-driven circulation system, the Atlantic meridional overturning cell (MOC), is a central element of the global thermohaline circulation (e.g., Gordon 1986; Broecker 1991) and a fundamental component of the global climate system. The strength of the Atlantic MOC has

important implications for the redistribution and sequestration of heat and climatically important atmospheric gases, and recent climate modeling efforts have demonstrated a strong relationship between the MOC and long-term climate transients (e.g., Manabe and Stouffer 1988; Street-Perrott and Perrott 1990; Jones 1991).

To accurately assess the role of the ocean circulation in modulating climate variability, a first-order description of the transport pathways that constitute the MOC and a general grasp of their relative significance are needed. Schmitz and Richardson (1991) found that almost one-half of the Florida Current transport is of South Atlantic origin, necessitating an interhemispheric and intergyre upper-ocean transport of about 14 Sv ( $\text{Sv} \equiv 10^6 \text{ m}^3 \text{ s}^{-1}$ ). Recent observational synthesis efforts (e.g., Schmitz and McCartney 1993; Schmitz 1996) have identified a number of transport pathways in the North Atlantic for the MOC return flow. The detailed description of these pathways has been hindered by a paucity of suitable observations, particularly in the low-latitude

\* Woods Hole Oceanographic Institution Contribution Number 9816.

*Corresponding author address:* Dr. David M. Fratantoni, Woods Hole Oceanographic Institution, Woods Hole, MA 02543.  
E-mail: dfratantoni@whoi.edu

Atlantic where time-dependent and three-dimensional transport processes are important. The tropical Atlantic exhibits a strong annual cycle forced by the annual migration of the intertropical convergence zone (e.g., Katz and Garzoli 1982; Katz 1987). In addition, the dominant low-latitude boundary current, the North Brazil Current (NBC), exhibits significant mesoscale variability (e.g., Metcalf 1968; Cochrane et al. 1979; Bruce et al. 1985; Johns et al. 1990, 1998). This variability, if unresolved by oceanographic measurement programs, can significantly affect our interpretation of the “mean” ocean circulation. For example, a northwestward coastal boundary current north of the NBC retroflexion (sometimes referred to as the Guiana Current) was generally thought to connect the equatorial region with the southeastern Caribbean (Sverdrup et al. 1942; Metcalf 1968). It is now believed that this description evolved largely as a result of the aliased measurement (rectification) of large and energetic North Brazil Current rings (Didden and Schott 1993; Richardson et al. 1994; Fratantoni et al. 1995) that transport South Atlantic water toward the Caribbean Sea.

In this study we employ a tropical-eddy-resolving<sup>1</sup> ocean circulation model to investigate the pathways by which the upper-ocean MOC return flow navigates the low-latitude Atlantic. The model is used to identify and quantify annual-mean return flow pathways and to examine the interplay between wind- and overturning-forced circulation systems. Although wind-forced seasonal variability in the tropical Atlantic is strong, we will focus on a description of the effective annual-mean circulation and the intensity and distribution of mesoscale variability. As will be described herein, the annual mean and mesoscale circulation patterns 1) exhibit a pronounced response to varying wind and overturning forcing, 2) are the most difficult to explore directly with present observational tools, and 3) are potentially the most relevant to understanding the MOC as a component of the climate system.

The remainder of this article is organized as follows. In section 2 the numerical model is described and details of its design, configuration, and forcing are presented. An overview of first-order model behavior and a comparison of a realistically forced simulation to the observed ocean circulation is offered in section 3. In section 4 we consider the impact of the MOC return flow on the mean and time-varying tropical Atlantic circulation, and in section 5 mass budgets are constructed to identify and quantify regional MOC transport pathways. Our results are summarized in section 6.

## 2. The numerical model

The U.S. Naval Research Laboratory’s layered ocean model (hereafter NLOM) was originally developed by

Hurlburt and Thompson (1980) for application to the Gulf of Mexico. With significant enhancements to code and capabilities (Wallcraft 1991; Shriver and Hurlburt 1997; Wallcraft and Moore 1997) the model has since been applied to physical oceanographic problems on regional, basin, and global scales. The basic features of the model can be summarized as follows. The model

- is a limited-area tropical Atlantic version of the NLOM with realistic coastline geometry and bottom topography,
- uses a small number of constant-density layers in the vertical to approximate the stratified ocean,
- solves vertically integrated nonlinear primitive equations for horizontal momentum and mass conservation using mass transport per unit width as the dependent variable,
- is purely hydrodynamic (does not incorporate thermodynamic equations for temperature and salinity) but does include a diapycnal mixing scheme,
- is forced by a combination of monthly climatological wind stress at the surface and steady imposed mass fluxes at partially open zonal boundaries.

### a. Model physics

The model equations consist of vertically integrated statements for the conservation of horizontal momentum and mass in each of  $n$  constant-density model layers, where  $n$  is typically  $\leq 6$ . These equations, their finite difference form, and the methods of their solution have been described at length by Hurlburt and Thompson (1980), Wallcraft (1991), Hurlburt et al. (1996), and Shriver and Hurlburt (1997). The simulations described here are strictly hydrodynamic, although thermodynamic versions of the model have been developed for other applications (e.g., Metzger et al. 1992; Heburn 1994). It is assumed that for the investigation of mass transport pathways, local thermodynamic forcing of the tropical Atlantic is of secondary importance relative to the effects of basin-scale surface wind stress and the global-scale MOC. Investigators with broader simulation goals have taken different approaches. For example, Philander and Pacanowski (1986) described a fully thermodynamic numerical model of the tropical Atlantic.

The surfacing of layer interfaces and the intersection of interfaces by submerged topography are difficult to deal with in a layer-oriented numerical model. Some contemporary numerical models handle this problem well. For instance, Bleck and Smith (1990) describe an isopycnal-coordinate model of the Atlantic Ocean in which layers may assume zero thickness anywhere within the domain, but at significant computational expense. In the NLOM layers are required to remain thicker than a specified threshold thickness (usually 40–50 m) everywhere within the model domain and bottom topography is not allowed to intersect any layer interface. This is computationally more efficient than layered

<sup>1</sup> The model is eddy resolving in tropical and low latitudes but only marginally so at midlatitudes.

TABLE 1. The vertical layer structure\* and imposed meridional mass fluxes\*\* used in the numerical model. Mass fluxes are positive northward. Each model layer roughly approximates an identifiable water mass in the tropical Atlantic Ocean. The rest thickness and depth correspond to a state of no motion. The thickness of model layer 6 varies with the bottom topography.

Model layer	Rest thickness (m)	Rest depth (m)	Interface $\sigma_t$	Layer $\sigma_t$	30°S flux (Sv)	47°N flux (Sv)	Approximate water mass
1	60	60	25.20	24.30	0.0	1.0	Surface
2	120	180	26.45	26.00	6.1	1.9	Thermocline/EUC
3	150	330	26.80	26.63	2.2	2.4	Lower Thermocline
4	300	630	27.20	27.03	3.9	4.7	Upper AAIW
5	450	1080	27.55	27.38	1.8	4.0	Lower AAIW
6	5420	6500		27.83	-14.0	-14.0	NADW

\* Model interfaces approximate commonly referenced watermass boundaries (e.g., Roemmich 1983; MacDonald 1993) and were defined as surfaces of constant density. Layer densities were determined by computing the domain-averaged density between the chosen interfacial surfaces using the Levitus (1982) climatology. The deepest model interface ( $\sigma_t = 27.55$ ) approximates the boundary between southward-flowing NADW and the most-dense component of the northward MOC return flow, AAIW. No distinction was made between NADW and Antarctic Bottom Water (AABW). In reality, northward flow of AABW partially compensates the southward export of NADW (McCartney and Curry 1993). In the model, the thick abyssal layer represents a vertical average of these two water masses.

\*\* Vertical transport structure was determined by combining the results of several basin-spanning geostrophic inverse calculations. At 30°S these included the work of Fu (1981), Rintoul (1991), and MacDonald (1993). The resulting transport profile was applied at inflow/outflow ports extending from the African coast to 0° (model layers 2–5) and at a narrow abyssal outflow port near the western boundary (model layer 6). The structure at 47°N was estimated using the observations of Wunsch and Grant (1982), McCartney and Talley (1984), and Roemmich (1980), and applied at a single port east of Flemish Cap. The top three model layers reach their minimum allowable thicknesses in the northern subtropical gyre (comparable to isopycnal outcropping). Because the stratification in these layers is dynamically insignificant (there are no local horizontal thickness gradients) the net outflow in layers 1–3 approximates the observed northward flow above  $\sigma_t = 26.80$ .

models<sup>2</sup> without these restrictions but limits high vertical resolution modeling to the upper ocean if realistic subsurface topography is used.

When a layer becomes thinner than a specified threshold thickness (usually 40–50 m), a “hydromixing” algorithm allows the localized transfer of mass and momentum between adjacent model layers (Wallcraft 1991). Specifically, mass from the next deepest layer is allowed to locally cross the interface separating the two layers. Compensation for this local diapycnal mixing via global (domainwide) detrainment to the layer below or via outflow through open model boundaries prevents mass accumulation in the entraining layer. Several methods for distributing this compensatory mass flux were investigated. While the manner in which this compensation is specified can affect the simulation, previous experiments indicated that the tropical circulation was generally insensitive to the choice of compensation scheme. In the experiments discussed herein, the global detrainment is distributed uniformly over the model domain. More detailed descriptions of the hydromixing algorithm and an alternative, nonspatially uniform detrainment scheme are presented in Shriver and Hurlburt (1997).

#### b. Model domain and boundary conditions

The tropical Atlantic model domain extends from 30°S to 47°N, with lateral boundaries defined by the

200-m isobath along continents and partially open zonal vertical walls at the northern and southern boundaries. The explicit exclusion of the North Atlantic subpolar gyre from the domain allowed formulation of a vertical layer/density structure expressly for the relatively shallow thermocline of the tropical ocean. Kinematic, no-slip boundary conditions are applied at all boundaries. Bottom topography is based on ETOP05 (NOAA 1986) with modifications in the Caribbean region by Youtsey (1993) and Hurlburt and Townsend (1994). The model equations were integrated on a staggered C grid (Mesinger and Arakawa 1976) with a resolution of 0.25° in latitude and 0.35° in longitude. A constant Laplacian horizontal eddy viscosity ( $A_H = 300 \text{ m}^2 \text{ s}^{-1}$ ) was specified.

#### c. Vertical structure and forcing

The model was configured with six isopycnal layers, five contained above a depth of  $\sim 1100$  m. Interfaces between model layers (defined as surfaces of constant density  $\sigma_t$ ) were chosen to approximately resolve thin equatorial currents such as the equatorial undercurrent (EUC). The high-velocity core of the EUC appears in layer 2, with additional eastward equatorial transport in the slightly denser layer 3. Layer densities and initial layer thicknesses are presented in Table 1.

Wind-forced experiments were driven with the monthly climatological wind stresses of Hellerman and Rosenstein (1983). Bryan et al. (1995) examined alternative wind climatologies for this region and found the Hellerman and Rosenstein stresses to produce the most reasonable low-latitude results. Surface stress is directly applied to the first model layer only. Lower model layers

<sup>2</sup> For the same vertical and horizontal resolution, the NLOM requires approximately one-tenth the computer time per model year as the Miami Isopycnal Coordinate Ocean Model (MICOM; Bleck and Smith, 1990; A. Wallcraft 1998, personal communication).

TABLE 2. Summary of numerical model experiments discussed in this article. The model was forced by the monthly Hellerman and Rosenstein (1983) and wind stress climatology (“wind”) and/or by a meridional overturning circulation (“MOC”) driven with specified inflow/outflow transport at partially open northern and southern model boundaries. The length of integration and analysis periods are given in model years.

Model expt	Wind forcing	MOC forcing	Integration length	Analysis length
A	Yes	No	100	15
B	No	Yes	136	3
C	Yes	Yes	100	15

are excited into motion by hydrostatically transmitted pressure forces resulting from the convergence and divergence of surface layer mass, by the vertical mixing of momentum, and by the imposition of mass fluxes at open boundaries. To simulate the global-scale MOC in this basin-scale model, mass fluxes were prescribed along partially open northern and southern domain boundaries. Following the recent observational summaries of Schmitz (1996) an MOC amplitude of 14 Sv was imposed. The zonal location and vertical structure of the prescribed mass fluxes were determined using available observations (see Table 1).

#### d. Experimental design

A suite of three numerical experiments (referred to as expts A, B, and C) are discussed in this article. These

experiments differ only in their forcing (Table 2). Experiments A and B isolate the wind and MOC forcing components, respectively, and are used to explore MOC interaction with the low-latitude wind-driven circulation. Experiment C is forced by a “realistic” combination of wind stress and a MOC, and is the focus of a model performance assessment in section 3. The three experiments were started from rest (zero velocity, flat model interfaces) and allowed to spin up to an approximate statistical equilibrium state as determined by the domain-averaged kinetic and potential energy. This required approximately 100 model years for the wind-driven experiments A and C and 136 years for experiment B. Approximately two Cray C90 processor hours were required for each year of model integration. The results presented here were synthesized from the final 15 years of integration for experiments A and C, and the final 3 years of integration for experiment B.

### 3. Overview of regional circulation and model behavior

Sverdrup (1947) postulated a steady, linear vorticity balance in the ocean interior between the meridional advection of planetary vorticity and the curl of the wind stress. This theory describes reasonably well the system of wind-driven gyres observed in the Atlantic Ocean, with boundaries between gyres defined by the location of vanishing wind stress curl (Fig. 1). Not shown in Fig.

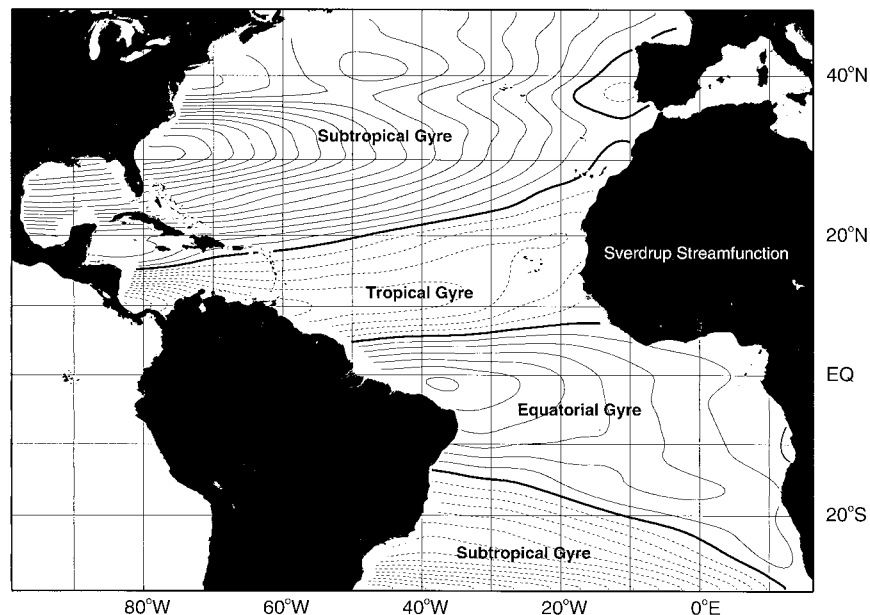


FIG. 1. Sverdrup streamfunction based on annual mean Hellerman and Rosenstein (1983) climatological wind stress. The contour interval is 2 Sv. Counterclockwise circulation is indicated by dashed contours. The boundaries between gyres are defined by the location of zero meridional Sverdrup transport and are indicated by bold contours. Four wind-driven gyres are contained within the model domain. The North Atlantic subtropical gyre, the tropical gyre, and the equatorial gyre are represented in their entirety. The South Atlantic subtropical gyre is truncated by the artificial southern domain boundary.

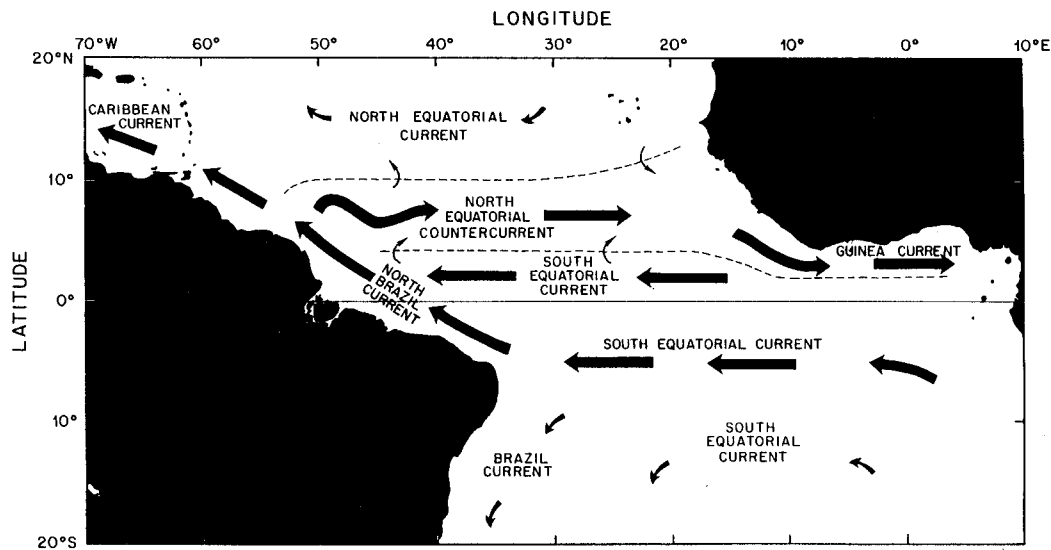


FIG. 2. A schematic of surface currents in the tropical Atlantic Ocean adapted from Richardson and Walsh (1986).

1 are the western boundary currents required to balance the interior meridional Sverdrup transport and provide a gyre closure. In the tropical Atlantic the dominant low-latitude western boundary current is the North Brazil Current, formed near  $10^{\circ}\text{S}$  from the bifurcation of the South Equatorial Current (SEC) on the coast of Brazil (Fig. 2). Recent analyses of climatological upper-ocean temperature fields (Molinari and Johns 1994) and synoptic observations (Bourles et al. 1999) indicate that the near-surface NBC retroflects (curves back upon itself) continuously throughout the year and maintains a consistent eastward flow into the western North Equatorial Countercurrent (NECC). The retroflecting NBC and its extension into the NECC form the boundary between the equatorial and tropical wind-driven gyres. The analyses presented in this article will focus on transport across and in the vicinity of this boundary.

In Fig. 3 we present an approximate streamfunction<sup>3</sup> for the annual-mean, vertically integrated upper-ocean transport in the realistically forced experiment C. The large-scale circulation patterns in this figure are grossly similar to those predicted by Sverdrup theory (Fig. 1) and include a compact, cyclonic tropical gyre separating the equatorial gyre and the northern subtropical gyre. The packed streamlines representing the mean NBC and NECC appear near  $5^{\circ}\text{--}8^{\circ}\text{N}$  and define the boundary between the equatorial and tropical gyres. The EUC is evident in the layer 1–5 streamfunction as a concentrated eastward flow along the equator and is not present

in the Sverdrup flow. Equatorial water that crosses the equatorial–tropical gyre boundary in a western boundary current enters the Caribbean through the Windward Island passages. This transport is augmented by additional equatorial water that has moved northward in the interior as part of the tropical gyre. The total westward transport through the Caribbean is composed of roughly equal parts northern- and southern-origin water, consistent with the composition of the Florida Current as reported by Schmitz and Richardson (1991).

Farther north in the subtropical gyre the modeled Gulf Stream does not separate from the coast at Cape Hatteras but instead follows the coastline to the northern domain boundary. The linear Sverdrup solution (Fig. 1) predicts two western boundary currents north of Cape Hatteras, one which separates from the coast and becomes a zonal jet, and another which continues northward along the coast. The  $\frac{1}{4}^{\circ}$  nonlinear model essentially shows a wiggly version of these linear pathways. Recent higher-resolution experiments with the NLOM show a more realistic Gulf Stream pathway (Hurlburt and Hogan 2000). Given the optimization of the model forcing and stratification for low-latitude applications, the poor simulation of Gulf Stream separation is neither surprising nor particularly relevant to the present study. A streamfunction for model layer 6 ( $\sigma_t > 27.55$ ; not shown) exhibits a narrow deep western boundary current (DWBC) similar to that described by Fine and Molinari (1988), flowing southward against the coasts of eastern North America, the Bahamas, the Lesser Antilles, and South America.

Several Atlantic Ocean variants of the NLOM have previously demonstrated reasonable performance when compared to observations. For example, Thompson et al. (1992) presented compelling comparisons between modeled and observed long-term transport time series

<sup>3</sup> Note that a streamfunction can only be formally defined if the flow is nondivergent. In all of our model experiments the annual mean diapycnal transport across the lowest model interface is small (generally less than  $0.2\text{ Sv}$ ). The nondivergence requirement is thus approximately satisfied when the entire upper ocean (layers 1–5;  $\sigma_t < 27.55$ ) is considered as a unit.

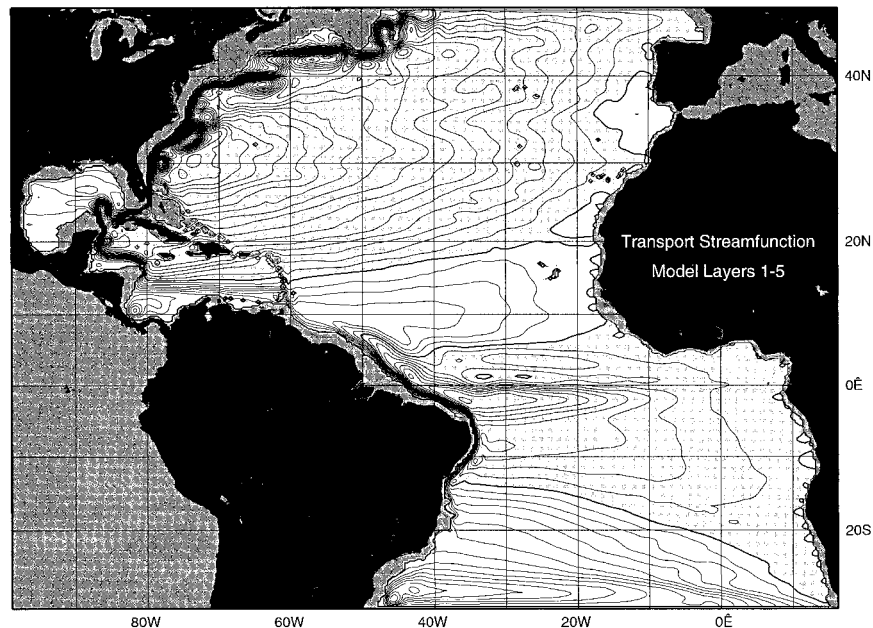


FIG. 3. Mass transport streamfunction for the vertically integrated flow above  $\sigma_t = 27.55$  (sum of model layers 1–5) for expt C, forced by winds and a MOC. The contour interval is 2 Sv. The flow is clockwise in shaded regions. Care must be taken when interpreting this figure as the circulation patterns indicated are not representative of flow within any single density interval. This is particularly significant in the equatorial Atlantic where the circulation is characterized by vertically layered currents and countercurrents.

in the Straits of Florida, and Hallock et al. (1989) reported favorable comparisons between modeled sea surface height variability, in situ observations, and satellite altimetry. Fratantoni et al. (1995) illustrated the ability of the NLOM to produce NBC rings similar to those observed. This ability is in contrast to other popular ocean models [including the Geophysical Fluid Dynamics Laboratory Tropical Atlantic Model (Philander and Pacanowski 1986) and the National Center for Atmospheric Research Community Climate Model (Holland and Bryan 1987), which do not exhibit realistic NBC rings (Johns et al. 1990; Didden and Schott 1993)]. Recently a very high resolution version of the Miami Isopycnic Coordinate Ocean Model has demonstrated a tendency to shed NBC ring-like features (E. Chassignet 1998, personal communication).

In the remainder of this section results from the “realistically forced” experiment C are briefly evaluated and compared with observations over a range of time-scales from the annual mean to the mesoscale. These comparisons suggest that conclusions drawn from this relatively simple numerical model have both qualitative and quantitative oceanographic relevance.

#### a. Annual mean transports

Constrained by topography and the subject of numerous measurement efforts, the Florida Current at 27°N has one of the best known transports in the World

Ocean. The Florida Current transport in experiment C (33.2 Sv) is in reasonable agreement with these observations (Table 3). Without an applied 14 Sv MOC (expt A) the modeled Florida Current transport decreases to 21.3 Sv in approximate agreement with the interior Sverdrup transport at 27°N (see Fig. 1). Note that all model-derived transports in Table 3 reflect the sum of model layers 1–5.

Farther south, recent moored velocity measurements in the NBC have resulted in reliable estimates of low-latitude western boundary current transport. The simulated transport in experiment C is generally consistent with these observations (Table 3). The small discrepancy between the observed and modeled transport could result from topographic effects (including the lack of a continental shelf and slope in the numerical model) and from the choice of offshore endpoint used as a limit of transport integration.

Most of the upper-ocean transport associated with the MOC enters the Caribbean Sea to join the Florida Current and the North Atlantic subtropical gyre system. According to Schmitz and Richardson (1991) and Wilson and Johns (1997), the dominant input of warm MOC return flow (i.e., water of South Atlantic origin) into the Caribbean is through the Windward Island passages, composed of the Grenada, St. Vincent, and St. Lucia passages in the southeastern Caribbean. The modeled annual mean transport through these passages in ex-

TABLE 3. Transports at selected locations in the tropical Atlantic as determined from numerical model experiments A–C and from observations. All transports shown are annual means with the exception of the equatorial undercurrent values that are from March. The model transport uncertainties (in parentheses) are standard deviations of 15-yr means for expts A and C, and 3-yr means for expt B. Model transports shown are the sum of model layers 1–5.

Geographic location	Expt A Wind-only	Expt B MOC-only	Expt C Wind + MOC	Observed value	Data source
Florida Current (27°N)	21.5 (2.1)	13.4 (1.0)	33.2 (2.6)	31.7 (3.0)	Leaman et al. (1987)
				32.5 (2.7)	Larsen (unpublished data) <sup>a</sup>
North Brazil Current (5°N) <sup>c</sup>	7.9 (5.3)	14.0 (1.4)	22.0 (7.0)	26 (7)	Johns et al. (1998)
Windward Island passages	−0.1 (1.5)	13.0 (0.8)	12.3 (1.3)	9.5 (3.0)	Wilson and Johns (1997) <sup>b</sup>
				25.1	Schmitz and Richardson (1991)
Equatorial undercurrent (40°W)	20.3 (13.6)	0.1 (4.3)	19.8 (13.3)	20.2	Schott et al. (1995)

<sup>a</sup> This value is a 7-yr mean derived from cable voltage measurements in the Florida Straits. See Larsen and Sanford (1985).

<sup>b</sup> The transport estimates offered by Wilson and Johns (1997) are derived from multiple repeat occupations using both hydrographic and direct velocity profiling, while those of Schmitz and Richardson (1991) result from the reanalysis of historical data, most notably that of Stalcup and Metcalf (1972). We believe the measurements of Wilson and Johns to be more reliable due to repeated sampling and the availability of statistical estimates of measurement uncertainty.

<sup>c</sup> Model values shown are the maximum transports achieved when meridional velocity is integrated in the offshore direction. This is a more consistent method of model intercomparison than choosing a fixed offshore endpoint, although it tends to weaken correspondence between model and observations.

periment C (Table 3) is in reasonable agreement with the observations of Wilson and Johns (1997).

Finally, Schott et al. (1995) measured the EUC transport at 40°W during March. The modeled mean transport for the same month, longitude, and in roughly the same

density class (eastward flow less dense than  $\sigma_t = 26.8$ ) compares favorably with this measurement (Table 3). The maximum velocity in the modeled EUC jet is 75–80  $\text{cm s}^{-1}$ , in good agreement with observations during GATE (e.g. Düing et al. 1980) and SEQUAL/FOCAL (Hisard and Henin 1984).

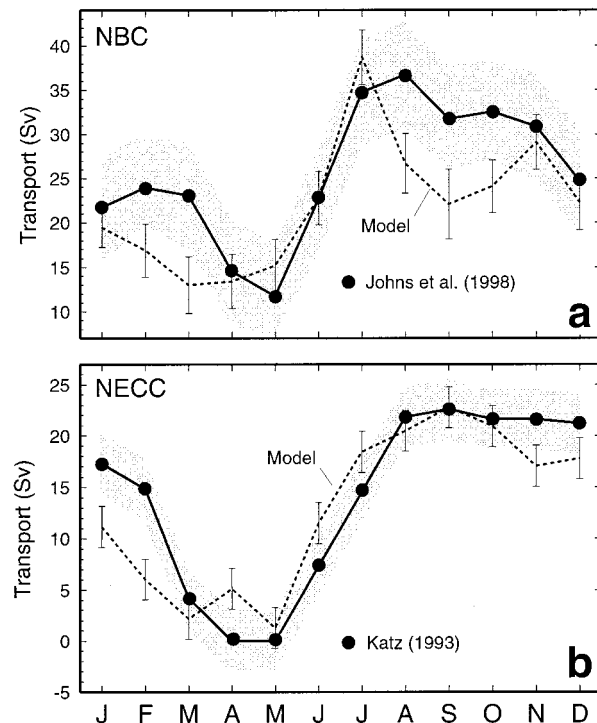


FIG. 4. Annual cycle of mass transport at two locations as determined from direct observation (solid line) and a numerical simulation (dashed line). (a) The North Brazil Current at 4°N from Johns et al. (1998) and expt C. (b) The North Equatorial Countercurrent at 38°W from Katz (1993) and expt C. Error bars are those specified by the investigator (for measured transports) or the standard error of estimated monthly means computed using 10 years of 3.05-day resolution numerical model output.

#### b. Annual transport cycles

Only a few locations in the low-latitude Atlantic have been observed for sufficient duration to confidently describe an annual transport cycle. Here we compare modeled and observed annual cycles at two such places: the NBC at 4°N and the NECC at 38°W. An annual cycle of NBC transport measured by Johns et al. (1998) is shown in Fig. 4a along with a similar record extracted from experiment C. The modeled maximum transport (38.7 Sv) is similar to the observed maximum of 36.8 Sv, and the total range of seasonal transport variation is well represented. The model successfully captures the sharp rise in transport in summer (May–July), which corresponds to the beginning of a period of strong NBC retroflection and maximum NECC transport. The transition periods just before and after this sharp rise are simulated least well by the model. Within the 6-Sv error bars estimated by Johns et al. (1998) the differences between the two series are only marginally significant.

Katz (1993) described long-term moored observations of the NECC at 38°W. Inverted echo sounders at 3°N and 9°N were used to estimate the meridional gradient in dynamic height over a period of almost 7 years. From this record we constructed an approximate time series of NECC transport (Fig. 4b). Agreement between experiment C and this time series is generally good, except during boreal winter when the modeled transport is somewhat lower than that observed.

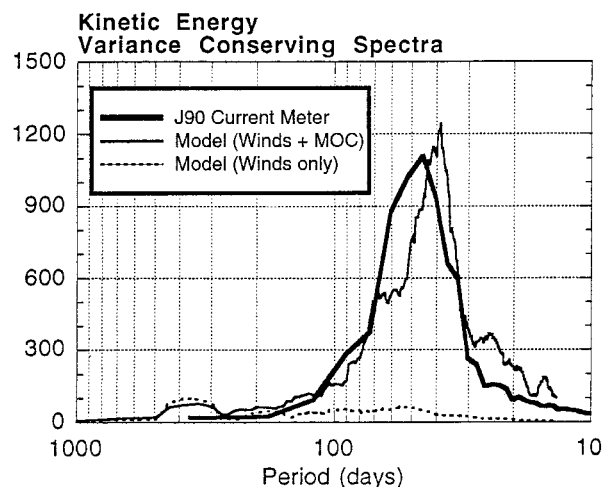


FIG. 5. Variance conserving kinetic energy spectra constructed from a velocity record at a nominal depth of 150 m at  $8.5^{\circ}\text{N}$ ,  $52.1^{\circ}\text{W}$  (from Johns et al. 1990; thick line) and at a similar location in the NLOM with (thin line) and without (dashed line) an imposed meridional overturning circulation. This figure was originally shown by Fratantoni et al. (1995).

### c. Eddy kinetic energy

In the western Atlantic, Pacific, and Indian Oceans, equator-crossing western boundary currents are modulated by 40–60 day period wavelike oscillations that can be as large as the mean flow (e.g., Mysak and Mertz 1984; Quadfasel and Swallow 1986; Ponte and Gutzler 1992; McClean and Klinck 1995). In addition to this variability, the NBC is known to shed large (400-km diameter) anticyclonic rings (e.g., Fratantoni et al. 1995) that transport South Atlantic water along the northeastern coast of South America toward the Caribbean Sea. In Fig. 5 we present a comparison of eddy kinetic energy (EKE) spectra from a velocity record obtained near the western boundary at  $8.5^{\circ}\text{N}$  (Johns et al. 1990) and from records extracted from model experiments similar to experiments A and C. Agreement between the observations and the realistically forced model experiment is good both in terms of amplitude and spectral content. Note the relatively low energy exhibited by the purely wind-forced experiment, particularly in the 30–70 day band corresponding to NBC ring generation. NBC rings are not formed in experiment A, suggesting a close relationship between the existence of the MOC and ring formation in the numerical model (see Fratantoni 1996). A common feature of spectral comparisons at other locations in the western low-latitude Atlantic is enhanced eddy energy in a model driven with combined wind and MOC forcing relative to one forced by winds alone. This point will be explored further in the next section.

## 4. The wind- and MOC-driven low-latitude circulation

Because the Atlantic circulation is driven in part by a source–sink system, the buoyancy-driven MOC, which

imposes a net meridional pressure gradient and demands northward upper-ocean transport, we expect dynamical differences between an ocean forced by winds alone and one forced by a combination of winds plus an overturning circulation. As will be demonstrated, these differences are sometimes more complex than would be expected from a simple superposition of overturning and wind-driven circulation modes.

### a. The vertically integrated circulation

In Fig. 6 we compare the mean low-latitude circulation patterns in experiments A, B, and C. A southward western boundary current along the northeast coast of South America closes the tropical gyre in experiment A and supplies fluid to the NECC and northward interior transport. There is no evidence of transport between the equatorial and tropical gyres, but rather a confluence of northern (tropical) and southern (equatorial) water near the NBC retroflection extending offshore into the NECC. Transport through the Windward Island passages recirculates cyclonically in an extension of the tropical gyre that fills the southern half of the Caribbean Sea. Flow entering the Caribbean north of Martinique passes through the Straits of Florida and recirculates within the North Atlantic subtropical gyre.

The dominant feature of the purely MOC-forced experiment B is a narrow and continuous northward-flowing western boundary current. After injection in the eastern South Atlantic, the imposed MOC return flow immediately shoots toward the western boundary, crosses the equator, and enters the Caribbean through the Windward Island passages. This flow continues through the Straits of Florida and exits the model domain through the partially open northern boundary. This behavior is, as expected, due to westward intensification as Rossby waves quickly confine the net meridional flow to the western boundary. The interior circulation is of very small amplitude and is not well organized.

The upper-ocean circulation in experiment C consists of both a continuous northward western boundary current and an interior wind-driven gyre circulation. The most significant difference between experiments A and C is the existence of intergyre mass transport in the latter. Most of the transport from the equatorial to the tropical gyre occurs in the western boundary layer, and the interior circulation is generally similar in form to that of the wind-forced experiment A. However, the source of fluid in the tropical gyre interior is not the same in each case. Rather than drawing water from the boundary current (as in expt A), a portion of the northward tropical gyre interior transport in experiment C is fed by South Atlantic (equatorial gyre) fluid leaving the coast in the retroflecting NBC. Further, while the tropical gyre is closed by a southward western boundary current in experiment A, a northward boundary current spanning the equatorial and tropical gyres is evident in experiment C. In general, the imposition of a northward

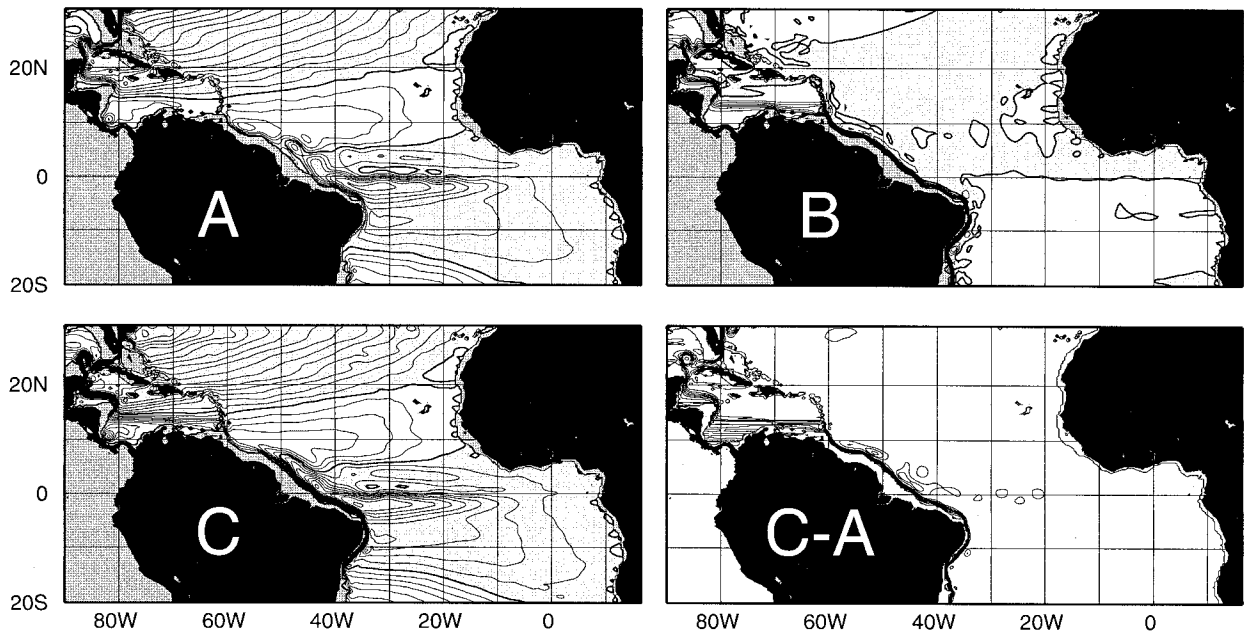


FIG. 6. As in Fig. 3, but for expts A, B, C, and the difference between expts C and A ("C - A").

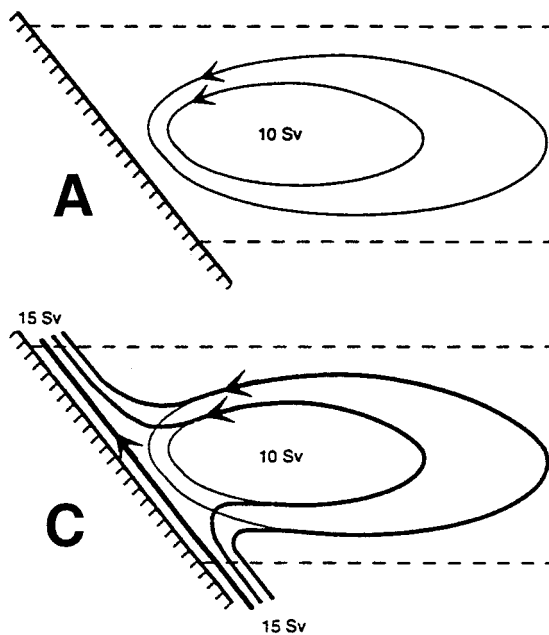


FIG. 7. Schematic of tropical gyre upper-ocean transport streamfunction for an ocean forced by (a) winds alone and (c) winds plus a net northward throughflow. Panels (a) and (c) approximate model expts A and C, respectively. The equatorial-tropical and tropical-subtropical gyre boundaries are approximated by the lower and upper dashed line, respectively. In the purely wind-forced case (a) the cyclonic tropical gyre requires a southward western boundary current to balance the northward interior Sverdrup transport. In (c) the interior Sverdrup transport is fed by a portion of the applied throughflow while the remainder flows northward in a western boundary current.

throughflow relaxes the requirement for a southward boundary current, as the northward interior Sverdrup transport can be fed from the south by the MOC throughflow rather than (or in addition to) recirculation from the western boundary current. This effect, previously recognized by Stommel (1960), is illustrated schematically in Fig. 7. Note that the South Atlantic subtropical gyre has the same behavior, except that the southward Brazil Current "survives" because it is stronger than the northward MOC.

A streamfunction for the transport difference between experiments A and C (Fig. 6) is generally similar to that of experiment B, suggesting that the vertically integrated annual-mean wind- and MOC-forced circulation modes can be superimposed in a nearly linear fashion. Deviations from this character are generally confined to the western boundary where small recirculation cells exhibit nonlinear enhancement when a MOC is imposed. The mean EUC jets in both experiments A and C exhibit several strong meanders. These meanders are of slightly different amplitude and phase and result in the additional structure along the equator in the C - A difference field. This characteristic is discussed further below.

#### b. Vertical structure of the mean circulation

As shown in Fig. 8, the dominant surface circulation features in experiments A and C are the retroflecting NBC, the NECC, the westward SEC, and the system of ridges and troughs associated with these currents. Compared to that in experiment A, the near-surface NBC in experiment C penetrates  $1^{\circ}$ - $2^{\circ}$  farther north before retroflecting. Other differences between experiments A

and C are most easily seen in the vector difference fields (labeled “C – A”) and consist of an enhanced anticyclonic recirculation within the NBC retroflexion and a weak residual northward flow along the South American continent. This residual northward flow generally resembles the surface circulation in the purely MOC-forced experiment B.

In the thermocline layer (a composite layer defined as the sum of model layers 2 and 3), the NBC separates from the coast to feed the EUC. As in the surface layer, the NBC in experiment C penetrates several degrees farther north in the thermocline before separation than in experiment A. Along the northeastern coast of South America direct subsurface measurements and model predictions indicate a thermocline depth coastal undercurrent (Wilson et al. 1994; Schott and Böning 1991). This undercurrent flows southeastward from the Windward Islands at a depth of around 150 m. It is strongly evident in experiment A, where it penetrates all the way to the equator to partially feed the EUC. However, in experiment C, it is weaker and separates from the coast north of the equator to feed the eastward North Equatorial Undercurrent [NEUC; Cochrane et al. (1979); visible near 5°N] and the EUC. Consistent with the downstream composition of the Florida Current as determined by Schmitz and Richardson (1991), which indicated no more than about 1 Sv of South Atlantic contribution to the thermocline layer transport, we find no significant northward transport of South Atlantic thermocline water beyond the latitude of the NBC retroflexion in either experiment A or C. The lack of a net northward flow at this depth does not preclude the possibility of a transient pathway for thermocline water in the western boundary layer, nor does it contradict observations of northward spreading of South Atlantic thermocline water properties (e.g., Worthington 1976) as isopycnal tracer mixing can occur independently of mass transport.

While EUC transports in both wind-driven experiments are nearly identical (Table 3), the EUC in experiment A is slightly narrower, is more intense (by about 5 cm s<sup>-1</sup>), and exhibits stronger meandering. The reason for these differences in EUC structure is not clear, although it may have to do with differences in the source waters for the EUC in the two experiments. A nearly symmetric confluence of northern and southern thermocline water on the equator in experiment A suggests that the meridional potential vorticity gradient across the western EUC might be strengthened relative to experiment C, in which the EUC source water is supplied primarily from the south. Such an enhanced gradient could contribute to a narrower and more intense EUC, and one more likely to exhibit instabilities and meandering behavior.

Interior circulation in a composite intermediate layer (the sum of model layers 4 and 5) is minimal in all three model experiments. A northward, equator-crossing intermediate western boundary current is evident in experiments B and C, but is absent in experiment A. This

boundary current, with speeds of 10–15 cm s<sup>-1</sup>, enters the Caribbean through the Windward Island passages. For comparison, Johns et al. (1990) found an annual mean northward velocity of 13 cm s<sup>-1</sup> at a depth of 900 m [within the Antarctic Intermediate Water (AAIW) and comparable in density to model layer 5] from moored current meter observations in the western boundary layer near 7.5°N.

The zonal structure of the low-latitude meridional western boundary flow at the equator and at latitudes 9°N and 9°S is summarized in Fig. 9. The most striking difference between experiments A and C is the reversal of the surface and intermediate boundary current near 9°N. Note also that the zonal scale of the boundary current jet does not change appreciably as transport in the western boundary layer varies between experiments. This suggests that the boundary current jet width in the numerical model is controlled primarily by lateral friction (e.g., Munk 1950). For the horizontal viscosity ( $A_H = 300 \text{ m}^2 \text{ s}^{-1}$ ) used in these simulations the Munk boundary layer scale  $(A/\beta)^{1/3}$  is approximately 25 km. The predicted width of the boundary current jet is  $(2\pi/3)^{1/2}$  times this value, or about 90 km. The jet widths depicted in Fig. 9 are about 100 km at the equator and slightly larger at 9°N and 9°S.

### c. Upwelling and water mass conversion

Westward winds drive a surface-layer Ekman transport divergence at the equator, resulting in the shoaling of the equatorial thermocline, upwelling, and the conversion of thermocline water to surface water. In drawing fluid from the thermocline into the surface layer, the wind-forced surface divergence drives a thermocline-layer equatorial convergence. This pattern is a fundamental feature of the wind-driven circulation and is not substantially altered by the presence of a mean MOC. However, depending on its vertical structure, the MOC can affect the equatorial symmetry of this pattern and the sources of thermocline water that supply the equatorial upwelling. The interaction of the MOC with the shallow, wind-driven equatorial overturning cell therefore has important consequences for the diapycnal conversion of the MOC return flow as it passes through the equatorial zone.

Figure 10 depicts the vertical structure of the mean, zonally integrated mass transport at 9°N and 9°S. The surface transport divergence and the thermocline convergence are evident in both experiments A and C and are of nearly equal magnitude. The annual mean upwelling from the thermocline to the surface is approximately 16 Sv in experiments A and C, in general agreement with previous observational (e.g., Roemmich 1983), climatological (e.g., Mayer and Weisberg 1983), and numerical (e.g., Philander and Pacanowski 1986) estimates.

In the purely wind-forced experiment A, the divergent surface flow and convergent thermocline flow is nearly

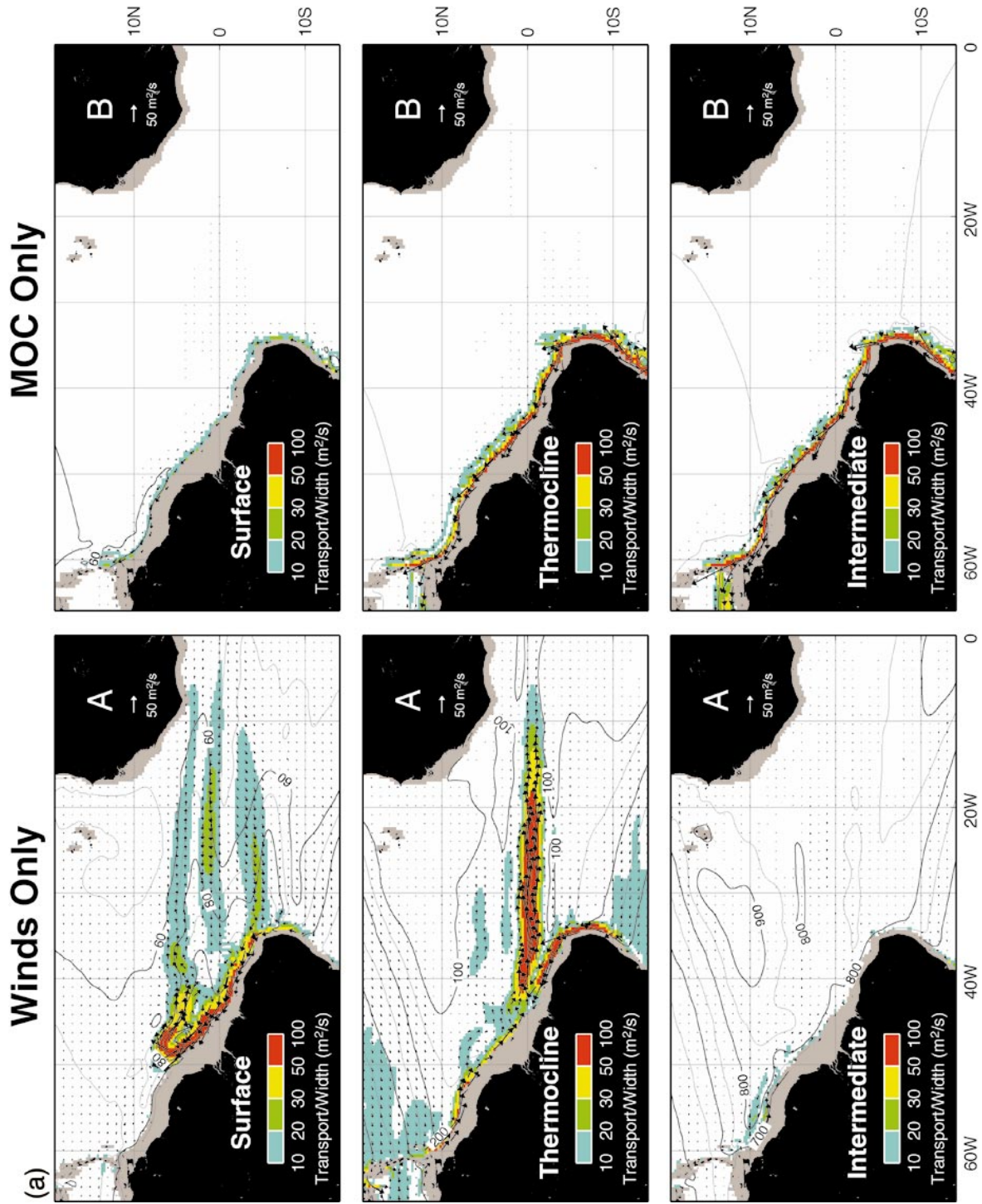


FIG. 8. Circulation within three density intervals: the surface layer (model layer 1), a composite thermocline layer (layers 2 + 3), and a composite intermediate layer (layers 4 + 5). Shown are annual-mean fields of thickness-weighted velocity (equivalent to transport per unit width) and layer thickness for expts A,

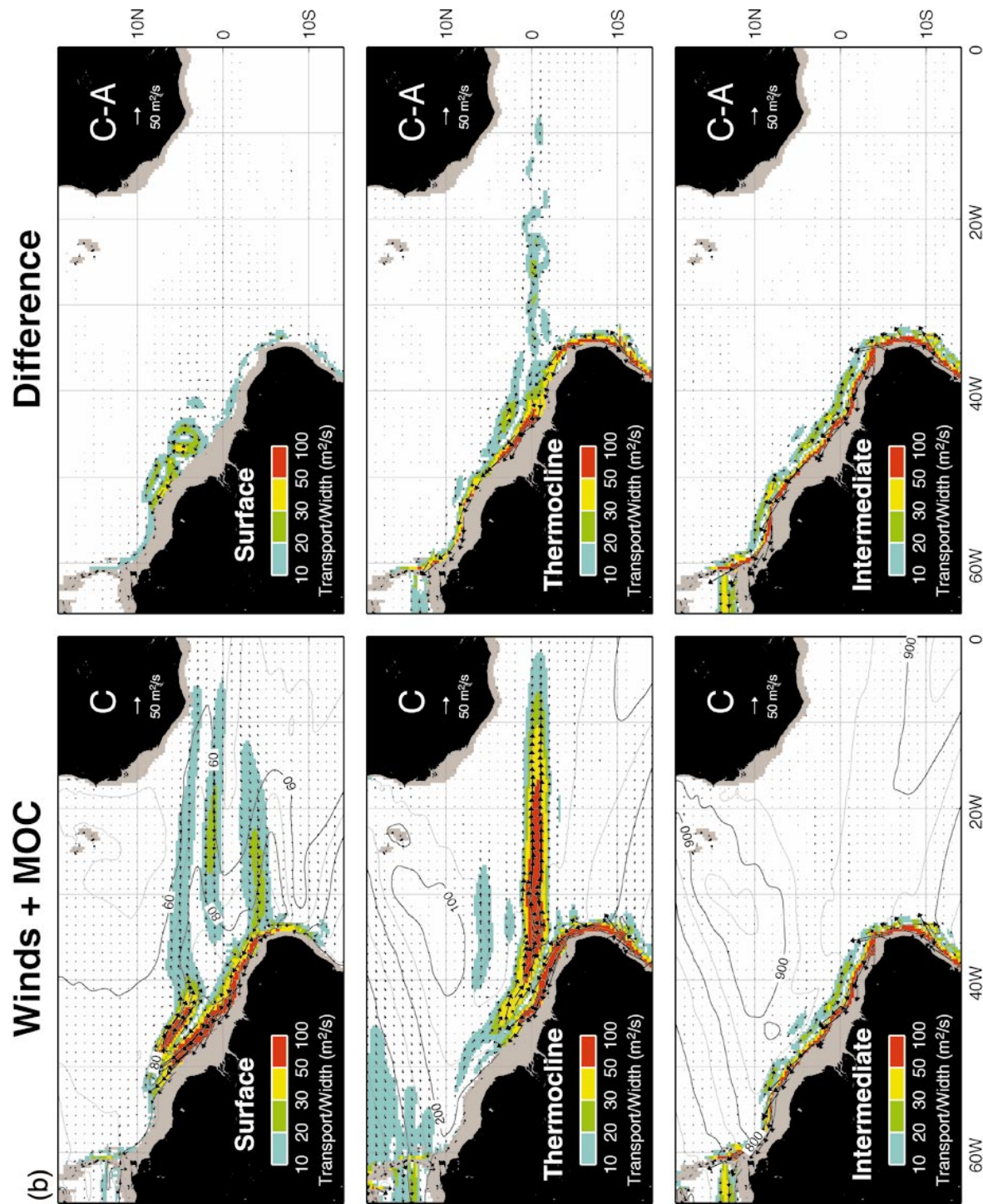


FIG. 8. (Continued) B, and C. Vectors indicate flow direction and intensity. Colors highlight areas of particularly strong flow. Layer thickness are contoured with an interval of 10 m (surface layer) and 50 m (thermocline and intermediate layers). The panel labeled "C - A" depicts the vector difference between expts C and A. Differences in layer thickness are not shown.

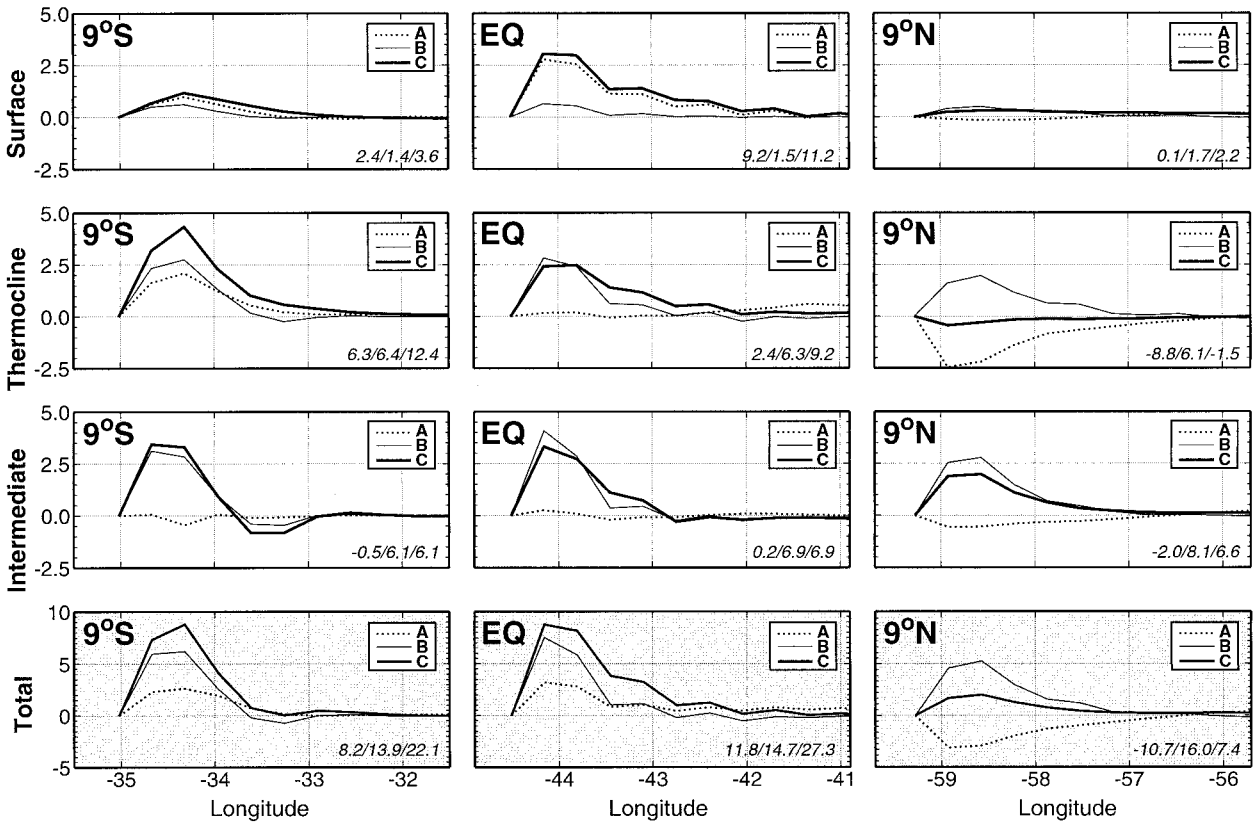


FIG. 9. A comparison of transport per unit width ( $m^2 s^{-1}$ ) near the western boundary as a function of longitude at three latitudes in the tropical Atlantic. Meridional transport structure is shown in four density intervals corresponding to model layers 1, 2 + 3, 4 + 5, and the total upper-ocean transport (1–5; shaded). The three numbers in the lower right corner of each panel indicate the integrated transport (in Sv, positive northward) in the western boundary region shown for expts A, B, and C. A summary of boundary versus interior transport is shown in Table 4.

symmetric about the equator (Fig. 10). However, in experiment C, the equatorward thermocline transport is highly nonsymmetric with mass being supplied mostly from the south. This supports the notion, previously recognized in the observations of Metcalf and Stalcup

(1967), that most of the water constituting the EUC in the western Atlantic is of South Atlantic origin. In experiment C, about 85% of the EUC transport at 40°W is of southern origin. This is significant, as the composition of the EUC largely determines the hemispheric

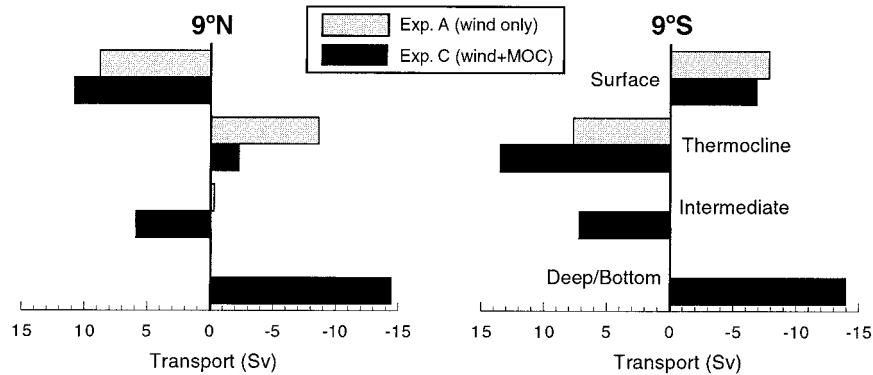


FIG. 10. Vertical structure of zonally integrated annual mean mass transport at 9°N and 9°S in the numerical model. Southward transport is toward the right. Transport is shown in four density intervals corresponding to model layers 1, 2 + 3, 4 + 5, and 6. Light and dark bars correspond to model expts A and C, respectively.

TABLE 4. Mean northward transport (in Sv) within surface (1), thermocline (2 + 3), and intermediate (4 + 5) model layers across latitudes 9°N and 9°S for expt C. The total meridional transport is divided into two sections, the western boundary and the ocean interior. The western boundary regime is defined as in Figure 9. Note particularly the strong hemispheric asymmetry of the equatorially convergent thermocline flow.

Model layer	9°N			9°S		
	W. boundary	Interior	Total	W. boundary	Interior	Total
1	2.2	8.4	10.6	3.6	-10.4	-6.8
2 + 3	-1.5	-1.0	-2.5	12.4	1.1	13.5
4 + 5	6.6	-0.8	5.8	6.1	1.0	7.1

origin of water transferred to the surface layer, at least in the western Atlantic. In experiment C, the equatorward thermocline transport across 9°N is almost equally divided between transport near the western boundary and in the ocean interior (Table 4). At 9°S, almost all of the equatorward transport is concentrated near the western boundary.

Intermediate and deep transport in the wind-forced experiment A is minimal, while the northward intermediate transport in experiment C changes only slightly between 9°S and 9°N, indicating little net diapycnal transport of intermediate water upward into the thermocline in the equatorial Atlantic. In a zonally averaged sense, the interaction of the MOC with shallow upwelling along the equator results in an enhanced upward conversion of South Atlantic thermocline water to surface water and a much reduced supply of North Atlantic water to the equatorial thermocline (Fig. 11). The fate of the upwelled South Atlantic water and the three-dimensional pathways of the MOC through the equatorial region are discussed in section 5.

#### d. Mesoscale variability and NBC ring generation

Earlier (Fig. 5) we noted a nonlinear increase in EKE near the western boundary when an MOC was added to an otherwise wind-driven model. This is demonstrated more clearly in Fig. 12, which shows the surface-layer western boundary transport at 9°N as a function of longitude and time. In experiment C, the variability is dominated by parallel northward/southward transport contours that move westward with time and are associated with large anticyclonic rings that pinch off from the NBC retroflexion (Johns et al. 1990; Fratantoni et al. 1995). Two to four of these rings are generated each year near 52°W and translate westward at 8–10 cm s<sup>-1</sup>. The period between successive ring passages at 9°N is about 50 days and the ring shedding exhibits a pronounced seasonality.

In experiment A, a single anticyclonic feature passes 9°N in late spring each year when the NBC transport decays to its minimum (see Fig. 4). Visual inspection of model snapshots (not shown) reveals this feature to

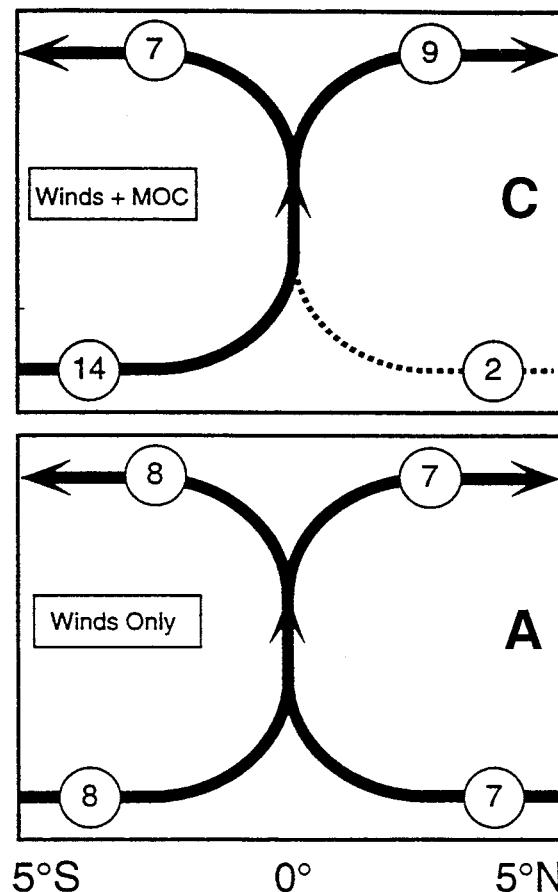


FIG. 11. Schematic illustrating the low-latitude conversion of thermocline water to surface water in the tropical Atlantic model. The vertically symmetric divergence (surface) and convergence (thermocline) in expt A yield no net interhemispheric mass transport. Thermocline water upwelled on the equator in expt C is primarily of southern origin. Hence net interhemispheric mass transport occurs even though wind-driven Ekman transport redistributes the upwelled water almost equally between hemispheres.

be a recirculation cell that escapes from the elbow of the retroflexion as the trade winds diminish and the NBC relaxes. This is quite different from the repeated shedding of NBC rings as represented in observations (e.g., Didden and Schott 1993; Fratantoni et al. 1995) and as modeled in experiment C. The anticyclonic features in experiment A are closely tied to the annual cycle and are relatively short lived, whereas those formed in experiment C persist much longer and are (most likely) generated as a result of instability processes related to the retroflexing NBC.

There is a small intermittent surface layer flow across 9°N in experiment B. About 1 Sv of thermocline water upwells into the surface layer in experiment B near the southern domain boundary and flows northward as a western boundary current. In the absence of wind forcing, the observed time-dependent transport across 9°N (mean period 42 days) must result from some form of instability related to the equator-crossing western

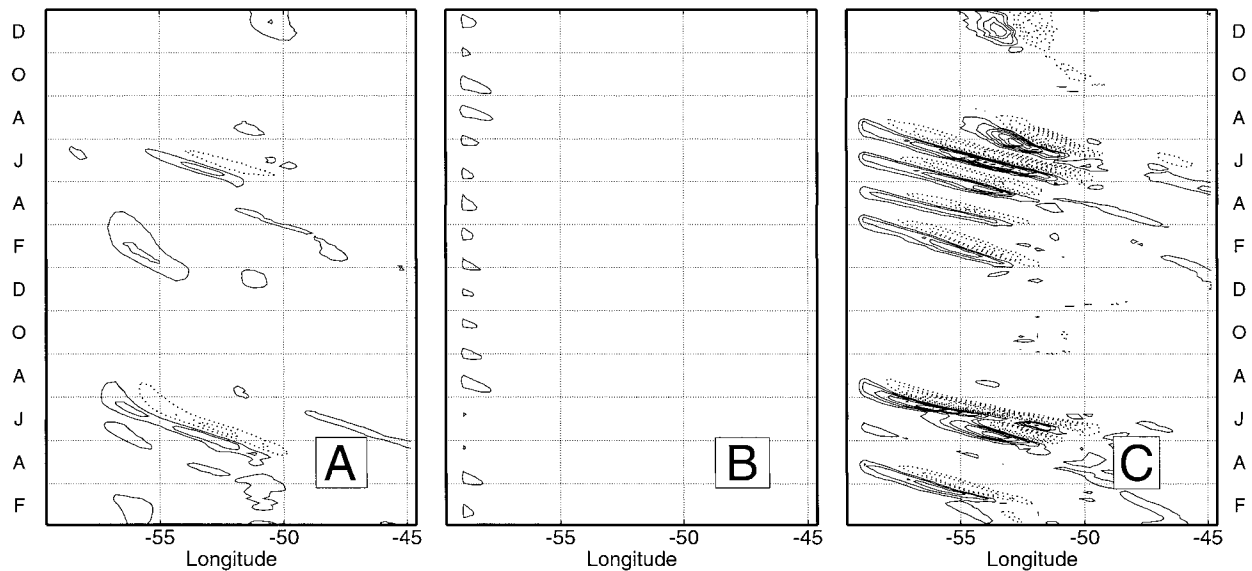


FIG. 12. Two-year time-longitude diagrams of meridional transport per unit width in the western boundary layer at  $9^{\circ}\text{N}$  for expts A, B, and C. Southward transport is dashed. Note the translation of 2–4 NBC rings per year past  $9^{\circ}\text{N}$  in expt C. Contour intervals is the same in each panel. The temporal resolution is 3.05 days.

boundary current. Similar behavior is not evident in experiment A or C.

Time series of surface-layer western boundary transport at  $9^{\circ}\text{N}$  (integrated over the zonal interval depicted in Fig. 12) are shown in Fig. 13a. The number and frequency of northward transport pulses associated with NBC ring passage are clearly greater in experiment C. Spectra of these time series are shown in Fig. 13b. Note the large 30–70 day peak in experiment C and the conspicuous absence of this peak in experiment A.

In addition to fundamental differences in NBC ring generation we find significant differences in the spatial distribution of mesoscale<sup>4</sup> EKE, particularly near the western boundary (Fig. 14). In both experiments A and C, and particularly in the C – A difference field, there is an obvious asymmetry of mesoscale variability about the equator. What physical mechanisms could be responsible for this asymmetry and for the enhancement of mesoscale variability in experiment C relative to experiment A? As mass transport in the western boundary layer is increased, so is the northward advection of low potential vorticity water of equatorial origin. The potential vorticity contrast between the boundary current and its surroundings is thus increased and could result in a state more favorable to the development of instabilities, which manifest themselves as mesoscale variability. Advection of waves and eddies from the equatorial waveguide into the western boundary layer (e.g.,

Carton 1992; Steger and Carton 1991) may also make a contribution to the enhanced mesoscale EKE along the South American coastline. Similarly, the generation and translation of North Brazil Current rings in experiment C tends to skew the distribution by extending a band of enhanced EKE along the western boundary as far as  $15^{\circ}\text{N}$ .

One explanation for the obvious nonlinear enhancement of mesoscale EKE in experiment C relative to experiment A may be relevant only within the framework of this numerical model. As described earlier, the width of the western boundary current is generally similar in all three model experiments (Fig. 9) and appears to be controlled by the imposed horizontal viscosity. The larger boundary current transport in experiment C results in a greater maximum jet velocity, larger horizontal shear, and the potential for increased generation of variability near the western boundary through lateral instability processes.

## 5. Low-latitude MOC return flow pathways

To diagnose low-latitude transport pathways within the tropical Atlantic model a mass budget subdomain comprising 13 control volumes was constructed between  $9^{\circ}\text{S}$  and  $9^{\circ}\text{N}$ . Composite annual cycles for each box face were computed from 15 years of model output for experiments A and C, and from 3 yr of output for experiment B. Philander and Pacanowski (1986) constructed a somewhat similar mass budget subdomain for their tropical Atlantic model, based on the primitive equation model of Bryan (1969). In the following we first discuss the movement of mass through the budget subdomain

<sup>4</sup> Here we differentiate mesoscale EKE from that due to seasonal fluctuations by applying a band-pass filter that retains only variability with periods of 10–100 days.

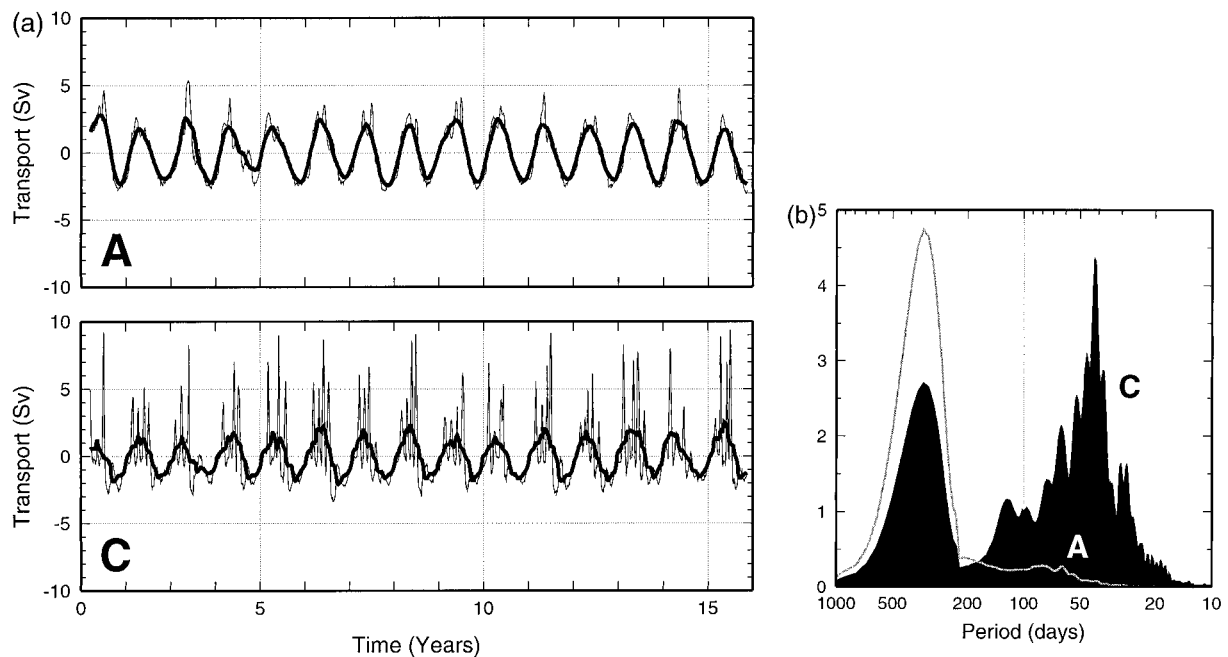


FIG. 13. (a) Time series of meridional western boundary transport at  $9^{\circ}\text{N}$  over a period of 15 years for expts A and C. A low-passed annual cycle is indicated by the bold line. Transport shown is the integral over the zonal interval depicted in Fig. 12. The mean annual transport has been subtracted in each panel. (b) Variance conserving meridional transport spectra corresponding to the time series in (a).

within the composite intermediate, thermocline, and surface layers (Fig. 15). Subsequently we focus on that portion of the mass transport that is directly related to the MOC return flow. The fractional transport due to the MOC is determined by comparing results from experiments A and C and by exploiting the property (described earlier) that the mean circulation can be approximated as a linear combination of wind-driven and MOC components. A schematic diagram that traces the upper-ocean MOC return flow through the equatorial zone including diapycnal water mass conversion pathways is shown in Fig. 16.

Model layers 4 and 5 approximate AAIW in the density interval  $26.80 < \sigma_t < 27.55$ . This corresponds to a range of potential temperatures of roughly  $5^{\circ}\text{--}12^{\circ}\text{C}$ . Schmitz and Richardson (1991) estimate that of the Florida Current transport in the  $7^{\circ}\text{--}12^{\circ}\text{C}$  temperature range, 83% (5 of 6 Sv) is of South Atlantic origin. This implies a relatively large transport of intermediate water across the equator, across the equatorial-tropical gyre boundary, and through the Caribbean Sea. In experiment C, 7.1 Sv of intermediate water enters the mass budget subdomain at  $9^{\circ}\text{S}$ , most of it within a 6.1 Sv intermediate western boundary current (Fig. 15a). A northward boundary current of similar magnitude leaves the subdomain at  $9^{\circ}\text{N}$ . There is no evidence of significant intermediate transport outside the western boundary layer at any latitude in the budget subdomain. Upwelling in the western equatorial Atlantic and beneath the NECC accounts for the net loss of approximately 1.2 Sv of intermediate water to the thermocline between  $9^{\circ}\text{S}$  and

$9^{\circ}\text{N}$ . This is somewhat smaller than the 3 Sv of intermediate water found by Roemmich (1983) to upwell into the lower thermocline between  $8^{\circ}\text{S}$  and  $8^{\circ}\text{N}$ . However, Roemmich (1983) also found a net throughflow of 7.4 Sv of AAIW at  $8^{\circ}\text{N}$ , comparable to our model result. Schott et al. (1995) offer an observation-based schematic of transport in the western tropical Atlantic, which agrees qualitatively with our conclusion that an intermediate western boundary current is the dominant intergyre transport pathway in this density class.

Model layers 2 and 3 ( $25.20 < \sigma_t < 26.80$ ) approximate the upper and lower portions of the main thermocline, and are similar to the  $12^{\circ}\text{--}24^{\circ}\text{C}$  temperature interval used by Schmitz and Richardson (1991). Less than 1 Sv of Florida Current transport in this temperature class is identified by Schmitz and Richardson as being of South Atlantic origin, compared to 7 and 5 Sv in the surface ( $>24^{\circ}\text{C}$ ) and intermediate ( $7^{\circ}\text{--}12^{\circ}\text{C}$ ) layers, respectively. Thermocline water injected along the equator in the EUC is upwelled into the surface layer, warmed, and redistributed by the surface layer circulation. The result is little or no interhemispheric or intergyre transport of unmodified South Atlantic thermocline water. In experiments A and C approximately 16 Sv of thermocline water converges on the equator between  $9^{\circ}\text{S}$  and  $9^{\circ}\text{N}$  and are converted to surface water (Fig. 15b). Of this amount, 13.6 Sv (85%) is Southern Hemisphere thermocline water in experiment C, but only 7.7 Sv (47%) is of southern origin in experiment A.

Mass budget diagrams for the surface layer are shown in Fig. 15c. Schmitz and Richardson (1991) estimate

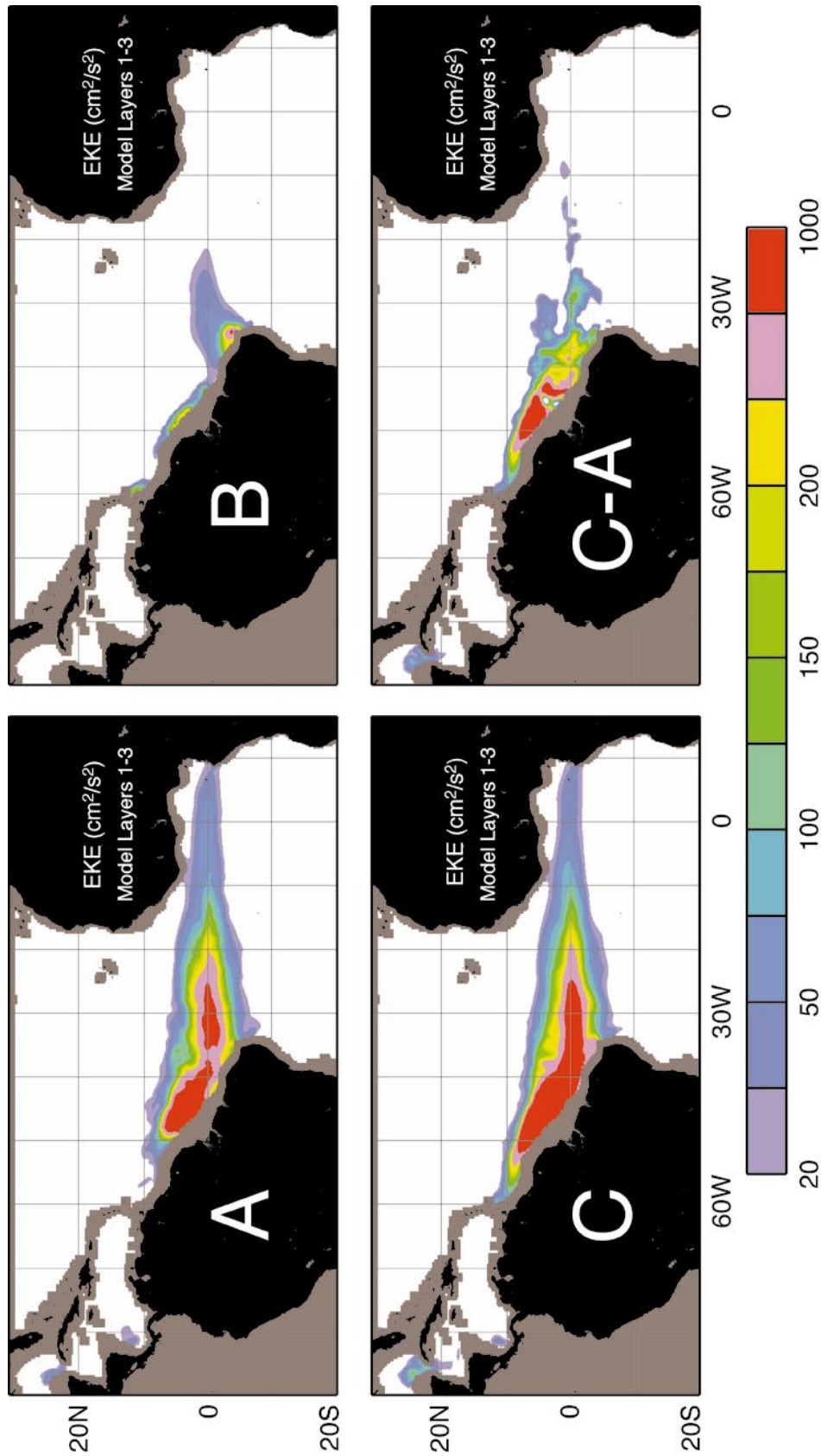


FIG. 14. Mesoscale (10–100 day period) eddy kinetic energy for the combined surface and thermocline layers of expts A, B, and C and for the difference between expts C and A. Note that the color scale is nonlinear.

that 7.1 Sv of South Atlantic water enters the Florida Current system at temperatures warmer than 24°C, a range roughly corresponding to model layer 1. Ekman transport redistributes the water upwelled along the equator to the north and south. Water transported southward meets the westward SEC and is swept into the boundary to join the equator-crossing NBC, while that transported northward continues to move through the ocean interior across the equatorial–tropical gyre boundary and into the NEC. Experiments with synthetic Lagrangian particles conducted as part of these numerical experiments indicate that an individual fluid parcel may circulate around the equatorial gyre several times before being transported northward into the tropical gyre. In an annual mean sense, the surface-layer transport at 9°N is almost equally divided between interior Ekman transport and the western boundary. Near the eastern boundary (not shown in detail) surface flow is generally to the south at latitudes south of 5°N and to the north at 9°N. This northward transport is consistent with a schematic of Mittelstaedt (1989), which suggests a bifurcation of the NECC at the African coast. In the numerical model, the small amount (less than 1 Sv) of surface water transported northward along the eastern boundary is not significant when compared to transport within the western boundary current. Fratantoni and Richardson (1999) have described SOFAR float observations of intermediate-depth flow suggestive of a northward-flowing low-latitude eastern boundary current and a potential intergyre transport pathway, but were unable to determine its transport.

The time-independent mass budget analysis presented here does not explicitly consider the transport contribution of NBC rings along the western boundary. Here they are simply included as part of the annual mean western boundary current transport. Evidence for separation of discrete mesoscale rings from the retroflecting NBC was first offered by Johns et al. (1990) in the form of Coastal Zone Color Scanner satellite imagery and moored current meter records. Annually, at least 2–4 rings are believed to translate from the NBC retroflection to the islands of the southeastern Caribbean where they disintegrate after a lifetime of about 100 days (Johns et al. 1990; Didden and Schott 1993; Richardson et al. 1994; Fratantoni et al. 1995). In experiment C an average of 3.4 rings are produced each year. As described by Fratantoni et al. (1995) the modeled rings are somewhat smaller and more surface trapped than those observed, resulting in an underestimate of ring transport in the numerical model as compared to available observations. In the model, NBC rings account for approximately 1.7 Sv of the net meridional transport in the western boundary versus approximately 3 Sv from observations. In the remainder of this study we therefore augment the numerical model results with our observational knowledge and assume that NBC rings are responsible for 3.0 Sv of surface layer transport. A more detailed discussion of the meridional transport associ-

ated with observed and modeled NBC rings is given by Fratantoni et al. (1995).

In summary, the model results suggest three major pathways for the transport of upper-ocean MOC return flow through the low-latitude Atlantic (Fig. 16). These are 1) an intermediate western boundary current, 2) western boundary transport in the surface layer including time-dependent NBC ring shedding, and 3) interior surface Ekman transport. These pathways are deduced from the mass budgets presented above and were confirmed with passive tracer distributions and Lagrangian drifter trajectories integrated along with the numerical model. In the intermediate layer 7.0 Sv of MOC return flow enters the low-latitude Atlantic. Approximately 1.0 Sv upwells through the thermocline and into the surface layer, leaving 6.0 Sv to continue into the North Atlantic. In the thermocline layer an additional 5.9 Sv of MOC return flow upwells to the surface layer near the equator. There is no net transport of MOC-related mass in the thermocline layer. In the surface layer, interior Ekman transport and transport within the western boundary layer (including NBC rings) move upwelled South Atlantic thermocline water north and south off the equator. That water transported southward is swept up in the westward SEC (2.7 Sv) to join 1.1 Sv that crosses the equator in the NBC. Of the total 3.8 Sv of surface-layer MOC return flow near the western boundary we assume (based on observational evidence) that approximately 3.0 Sv is due to transient NBC rings. Thus in reality only a small (less than 1 Sv) portion of the surface western boundary transport may take place as a continuously connected western boundary current. The remaining MOC surface water (4.2 Sv) moves northward via interior Ekman transport across the NECC and into the tropical gyre. Overall the three pathways, 1), 2), and 3) above, are of roughly equal importance to the net transport of 14 Sv of MOC return flow through the low-latitude Atlantic.

## 6. Summary and conclusions

In this article we described an investigation of the annual mean and mesoscale circulation in the low-latitude Atlantic Ocean and demonstrated that a relatively simple numerical model of the tropical Atlantic reasonably simulates key aspects of the observed low-latitude circulation. Comparison of numerical experiments forced with and without an imposed MOC revealed significant differences in circulation patterns near the low-latitude western boundary, particularly in the thermocline and intermediate layers. We found that, in an annual mean sense, the large-scale circulation in a model ocean forced by both surface wind stress and an applied meridional overturning cell can be well approximated by a linear superposition of wind- and overturning-forced solutions [as recognized first by Stommel (1960)] even though localized nonlinearity in the form of diapycnal mixing is essential to portions of the mean MOC

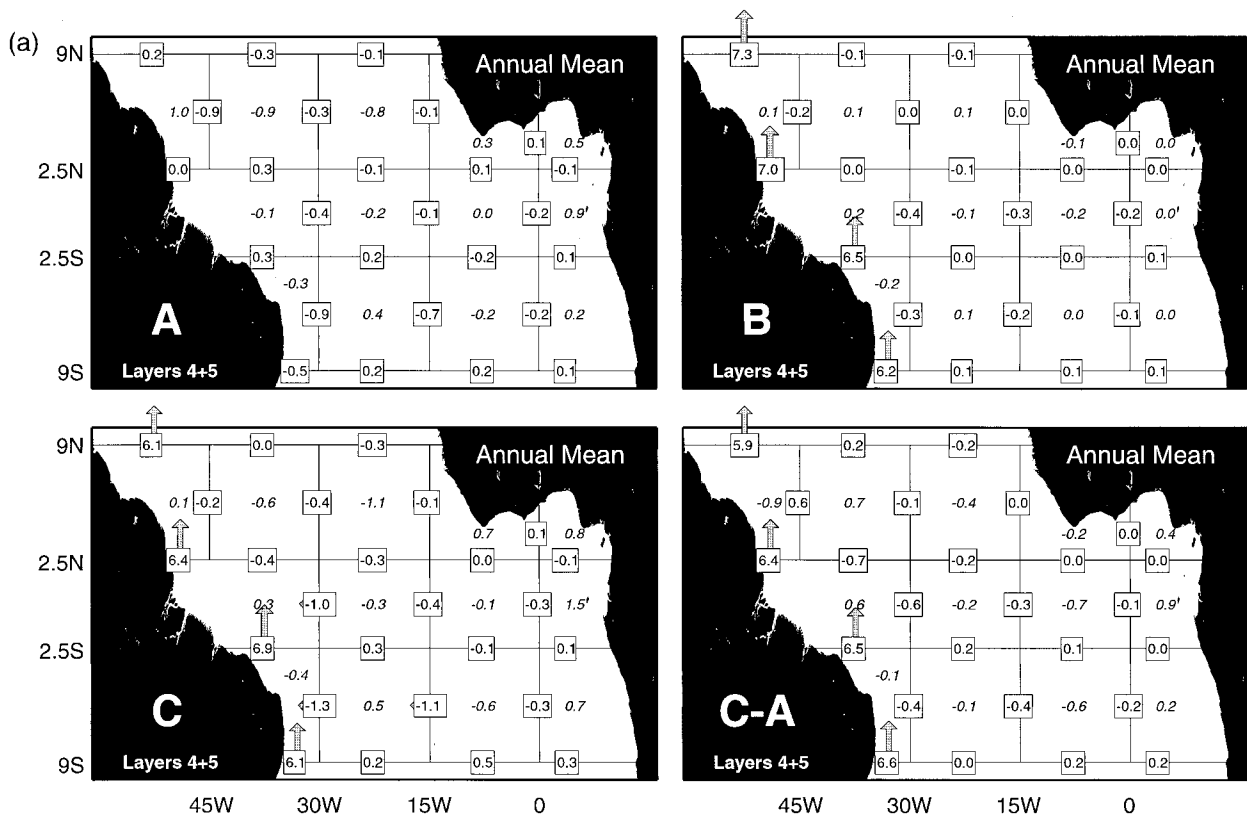


FIG. 15. Annual-mean mass budget diagram for the (a) intermediate, (b) thermocline, and (c) surface layers of expts A, B, C. Also shown is the difference between expts C and A ( $C - A$ ) in each composite layer. Arrows and boxed numbers indicate isopycnal transport magnitude (positive north, east). The italicized number in the center of each control volume indicates vertical (diapycnal) transport (positive up) across the lower interface of the control volume.

pathway. While annual mean transport magnitudes may combine linearly, significant changes were found in Lagrangian transport pathways. For example, we demonstrated that the source of fluid to support northward interior Sverdrup transport in the cyclonic tropical gyre changes from a southeastward gyre-closing boundary current (in a purely wind-forced simulation) to a portion of the northward MOC return flow (in a simulation including an overturning cell). A fundamental change was also noted in the hemispheric source of water feeding the equatorial undercurrent. In a purely wind-driven experiment the water injected along the equator is almost equally partitioned between northern (tropical gyre) and southern (equatorial gyre) water, while an experiment forced with both winds and a MOC results in an equatorial undercurrent that is predominantly fed from the south, consistent with in situ observations (e.g., Metcalf and Stalcup 1967).

At higher frequencies, particularly within a mesoscale band of 10–100 day period, the intensity of variability along the low-latitude western boundary is significantly and nonlinearly enhanced in a model forced by a combination of winds and a meridional overturning cell, relative to a model forced by winds alone. This enhancement is thought to result from a combination of

instability processes driven by enhanced horizontal shear and an enhanced potential vorticity gradient and by advection of vorticity from the equatorial waveguide by the NBC. Additional differences in mesoscale EKE north of the equatorial–tropical gyre boundary can be attributed to the formation and propagation of NBC rings in experiment C. Our finding that NBC rings are not formed in a purely wind-driven simulation (expt A) is an extreme example of the nonlinear response to increased transport in the low-latitude western boundary current resulting from the addition of a MOC. One important question (and one not addressed with the present set of numerical experiments) is the difference in dynamical response to the addition of a MOC versus an increase in the strength of wind forcing. If the noted differences in circulation character are purely a result of increased western boundary current transport (and not specifically related to cross-equatorial or intergyre transport), then an increase in wind stress curl may evoke the same response.

We identified three main pathways for the transport of the upper-ocean MOC return flow through the low-latitude Atlantic. Interior surface Ekman transport, surface transport in the western boundary layer (including time-dependent NBC ring shedding), and an interme-

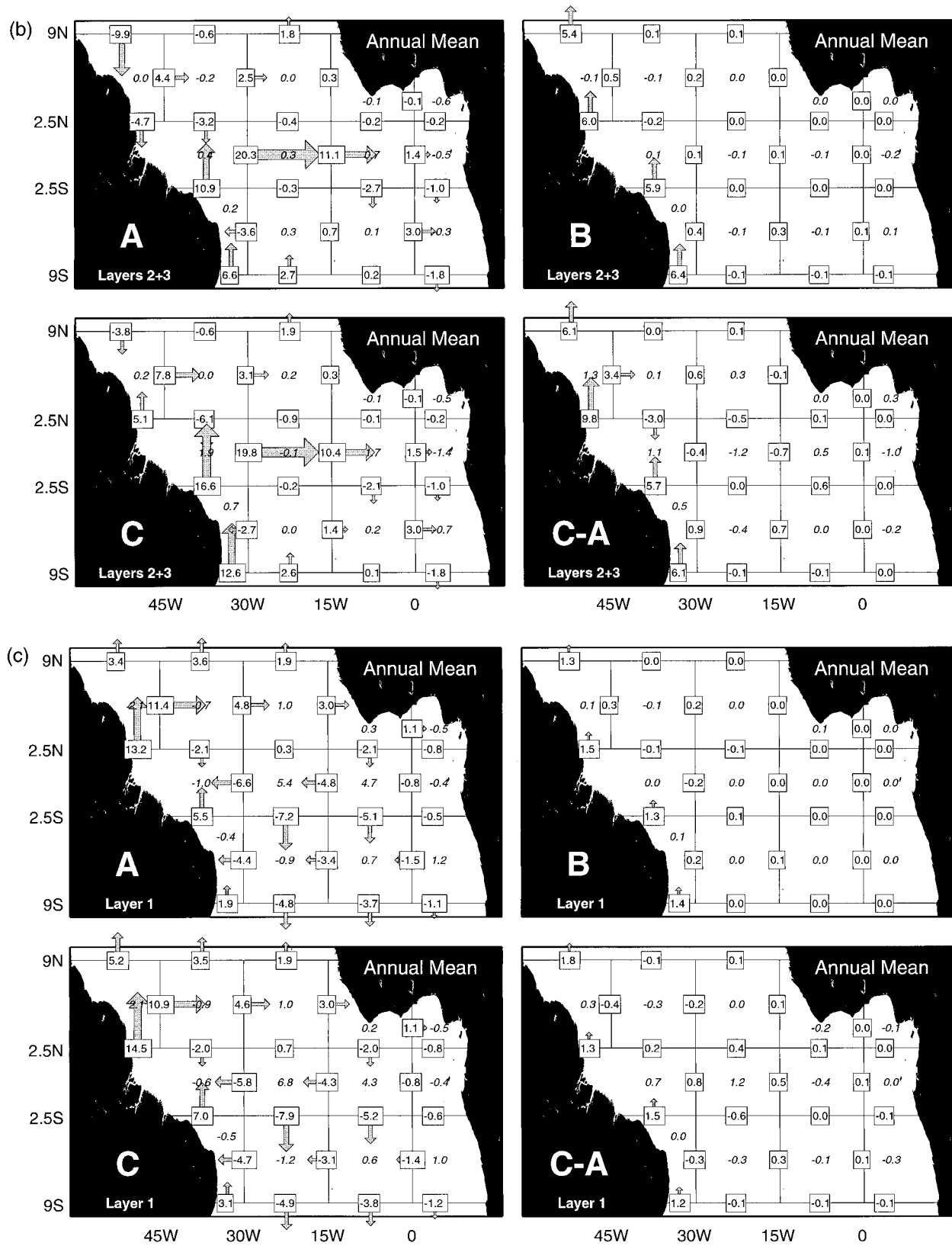


FIG. 15. (Continued)

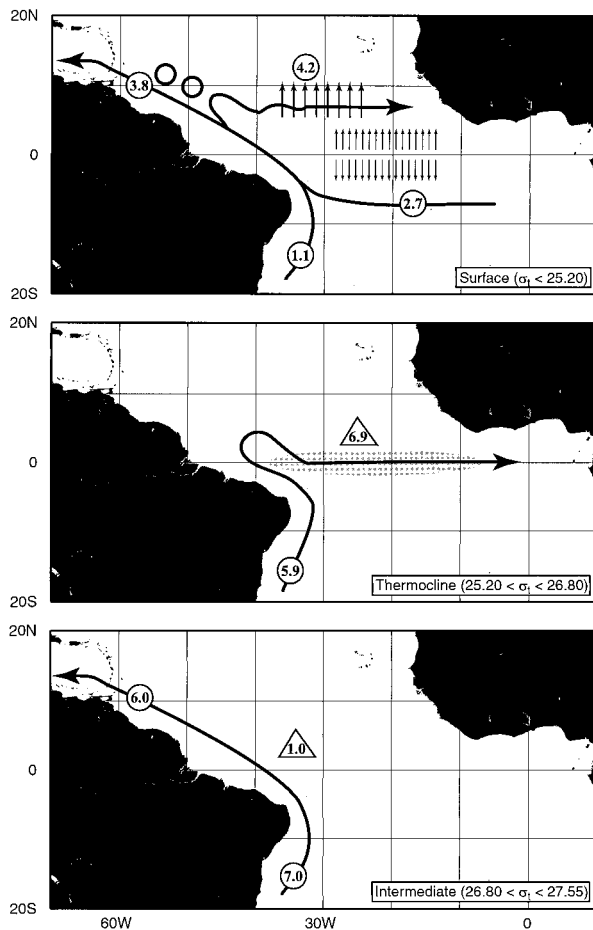


FIG. 16. Schematic summary diagram depicting the effective annual-mean MOC return flow pathways within the surface, thermocline, and intermediate layers. Solid line indicates the dominant route for MOC return flow in each density interval with mass transport (Sv) values as indicated. Significant upwelling regions are identified by shaded areas with transports (Sv) shown within the triangles. Note that this diagram depicts *only* that transport associated with the MOC return flow.

diate western boundary current were all found to be important to the annual-mean return flow transport of 14 Sv. In contrast to transport schematics presented by Schmitz and McCartney (1993) and Schmitz (1996) the model indicates no net meridional transport of intermediate water in the low-latitude interior away from the western boundary. Rather, the dominant annual mean pathway of intermediate water through the low-latitude Atlantic is an intermediate western boundary current along the northeast coast of South America. While there is some observational evidence of such a flow (e.g., Johns et al. 1990) additional in situ measurements are necessary to verify the characteristics of this circulation feature.

What role does the low-latitude wind-driven circulation play in determining the global-scale meridional overturning circulation? Are there reasonable scenarios in which changes in low-latitude wind forcing could

induce climatically significant large-scale changes in the Atlantic basin? The magnitude of the MOC is set by high-latitude sinking and interior mixing processes and is not first-order controlled or dictated by the mechanisms of intergyre transport discussed herein. Rather, the low-latitude wind-driven circulation acts to modify the vertical structure of the warm return flow to the North Atlantic. The results of this investigation suggest that the low-latitude wind-driven circulation strongly modifies the vertical structure and transport pathways of the upper-ocean MOC return flow. Processes in the low-latitude Atlantic set the initial state of the MOC return flow upon its entrance into the North Atlantic and define the vertical density structure of water entering the Caribbean, the Straits of Florida, and the North Atlantic subtropical gyre. Equatorial upwelling, in particular, converts a large amount of South Atlantic thermocline water to surface water, fundamentally changing the stratification of the upper-ocean MOC. Atmospheric interaction (cooling and evaporation) in the subtropical and subpolar gyres is responsible for setting the final thermodynamic state of surface water and initiating deep-water formation. While other areas of the global ocean also make fundamental contributions to the water mass characteristics of the upper-limb of the MOC, that of the low-latitude Atlantic is the final and most dramatic before the long stretch of surface evaporation and cooling in the subtropical gyre leading up to high-latitude convection. Studies using models with active thermodynamics as well as additional observations are needed to further quantify the role of the low-latitude Atlantic in the global climate system. The extent to which interannual changes in low-latitude wind forcing may affect diapycnal water mass conversion and MOC throughflow pathways, and the potential impact of these changes on deep-water formation processes, are topics in need of further study.

*Acknowledgments.* Support for D.M.F. during preparation of this manuscript was provided by the National Science Foundation through Grant OCE91-14656 and by the National Oceanic and Atmospheric Administration through Subcontract 40AANE809079. W.E.J. gratefully acknowledges support from the Office of Naval Research through Contract N00014-95-1-0025 and from the National Science Foundation through Grant OCE-9730322. T.L.T. and H.E.H. were supported by the project "Dynamics of Low-Latitude Western Boundary Currents" funded by the Office of Naval Research under Program Element 61153N. Model integration was performed on a Cray C90 at the Naval Oceanographic Office, Stennis Space Center, Mississippi, a component of the Department of Defense High Performance Computing Initiative. We thank P. L. Richardson and two anonymous reviewers for comments and suggestions which improved this manuscript.

## REFERENCES

- Bleck, R., and L. T. Smith, 1990: A wind-driven isopycnic coordinate model of the north and equatorial Atlantic Ocean I: Model development and supporting experiments. *J. Geophys. Res.*, **95**, 3273–3285.
- Bourles, B., R. L. Molinari, E. Johns, W. D. Wilson, and K. D. Leaman, 1999: Upper layer currents in the western tropical North Atlantic (1989–1991). *J. Geophys. Res.*, **104**, 1361–1375.
- Broecker, W. S., 1991: The great ocean conveyor. *Oceanography*, **4**, 79–89.
- Bruce, J. G., J. L. Kerling, and W. H. Beatty III, 1985: On the North Brazilian eddy field. *Progress in Oceanography*, Vol. 14, Pergamon, 57–63.
- Bryan, F. O., I. Wainer, and W. R. Holland, 1995: Sensitivity of the tropical Atlantic circulation to specification of wind stress climatology. *J. Geophys. Res.*, **100**, 24 729–24 744.
- Bryan, K., 1969: A numerical method for the study of the circulation of the world ocean. *J. Comput. Phys.*, **4**, 347–376.
- Carton, J. A., 1992: Tropical Atlantic eddies collide with the coast of South America (abstract). *Eos, Trans. Amer. Geophys. Union*, **72** (51), 22.
- Cochrane, J. D., F. J. Kelly, and C. R. Olling, 1979: Subthermocline countercurrents in the western equatorial Atlantic Ocean. *J. Phys. Oceanogr.*, **9**, 724–738.
- Didden, N., and F. Schott, 1993: Eddies in the North Brazil Current retroflection region observed by GEOSAT altimetry. *J. Geophys. Res.*, **98**, 20 121–20 131.
- Düing, W., F. Ostapoff, and J. Merle, 1980: *Physical Oceanography of the Tropical Atlantic during GATE*. University of Miami, 117 pp.
- Fine, R. A., and R. L. Molinari, 1988: A continuous deep western boundary current between Abaco (26.5N) and Barbados (13N). *Deep-Sea Res.*, **35**, 1441–1450.
- Fratantoni, D. M., 1996: On the pathways and mechanisms of upper-ocean mass transport in the tropical Atlantic Ocean. University of Miami/RSMAS Tech. Rep. RSMAS-96-006, 250 pp. [Available from Rosenstiel School of Marine and Atmospheric Science, 4600 Rickenbacker Causeway, Miami, FL 33149.]
- , and P. L. Richardson, 1999: SOFAR float observations of an intermediate-depth eastern boundary current and mesoscale variability in the eastern tropical Atlantic Ocean. *J. Phys. Oceanogr.*, **29**, 1265–1278.
- , W. E. Johns, and T. L. Townsend, 1995: Rings of the North Brazil Current: Their structure and behavior inferred from observations and a numerical simulation. *J. Geophys. Res.*, **100**, 10 633–10 654.
- Fu, L., 1981: The general circulation and meridional heat transport of the subtropical South Atlantic determined by inverse methods. *J. Phys. Oceanogr.*, **11**, 1171–1193.
- Gordon, A. L., 1986: Inter-ocean exchange of thermocline water. *J. Geophys. Res.*, **91**, 5037–5046.
- Hallock, Z. R., J. L. Mitchell, and J. D. Thompson, 1989: Sea surface topographic variability near the New England Seamounts: An intercomparison among in-situ observations, numerical simulations, and GEOSAT altimetry from the Regional Energetics Experiments. *J. Geophys. Res.*, **94**, 8021–8028.
- Heburn, G. W., 1994: The dynamics of the seasonal variability of the western Mediterranean circulation. *Seasonal and Interannual Variability of the Western Mediterranean Sea*, P. E. La Violette, Ed., Coastal Estuarine Studies, Vol. 46, Amer. Geophys. Union, 249–285.
- Hellerman, S., and M. Rosenstein, 1983: Normal monthly wind stress over the world ocean with error estimates. *J. Phys. Oceanogr.*, **13**, 1093–1104.
- Hisard, P., and C. Henin, 1984: Zonal pressure gradient, velocity, and transport in the Atlantic equatorial undercurrent from FOCAL cruises (July 1982–February 1984). *Geophys. Res. Lett.*, **11**, 761–764.
- Holland, W. R., and F. Bryan, 1987: Progress in the WOCE Ocean Community Modeling Effort (abstract). *Eos, Trans. Amer. Geophys. Union*, **68**, 1311.
- Hurlburt, H. E., and J. D. Thompson, 1980: A numerical study of Loop Current intrusions and eddy shedding. *J. Phys. Oceanogr.*, **10**, 1611–1651.
- , and T. L. Townsend, 1994: NRL effort in the North Atlantic, data assimilation and model evaluation experiments—North Atlantic Basin: Preliminary experiment plan, Center for Ocean and Atmospheric Modeling (COAM), University of Southern Mississippi. Rep. PR-2-9S, 50 pp. [Available from University of Southern Mississippi/COAM, Stennis Space Center, MS 39529.]
- , and P. J. Hogan, 2000: Impact of 1/8° to 1/64° resolution on Gulf Stream model-data comparisons in basin-scale subtropical Atlantic Ocean models. *Dyn. Atmos. Oceans*, in press.
- , A. J. Wallcraft, W. J. Schmitz Jr., P. J. Hogan, and E. J. Metzger, 1996: Dynamics of the Kuroshio/Oyashio current system using eddy-resolving models of the North Pacific Ocean. *J. Geophys. Res.*, **101**, 941–976.
- Johns, W. E., T. N. Lee, F. A. Schott, R. J. Zantopp, and R. H. Evans, 1990: The North Brazil Current retroflection: Seasonal structure and eddy variability. *J. Geophys. Res.*, **95**, 22 103–22 120.
- , —, R. Beardsley, J. Candela, and B. Castro, 1998: Annual cycle and variability in the North Brazil Current. *J. Phys. Oceanogr.*, **28**, 103–128.
- Jones, G. A., 1991: A stop-start ocean conveyor. *Nature*, **341**, 364–365.
- Katz, E. J., 1987: Seasonal response of the sea surface to the wind in the equatorial Atlantic. *J. Geophys. Res.*, **92**, 1885–1893.
- , 1993: An interannual study of the Atlantic North Equatorial Countercurrent. *J. Phys. Oceanogr.*, **23**, 116–123.
- , and S. Garzoli, 1982: Response of the western equatorial Atlantic Ocean to an annual wind cycle. *J. Mar. Res.*, **40**, 307–329.
- Larsen, J. C., and T. B. Sanford, 1985: Florida Current volume transports from voltage measurements. *Science*, **227**, 302–304.
- Leaman, K. D., R. L. Molinari, and P. S. Vertes, 1987: Structure and variability of the Florida Current at 27°N: April 1982–July 1984. *J. Phys. Oceanogr.*, **17**, 565–583.
- Levitus, S., 1982: *Climatological Atlas of the World Ocean*. NOAA Prof. Paper No. 13, U.S. Govt. Printing Office, Washington, D.C., 173 pp.
- MacDonald, A. M., 1993: Property fluxes at 30°S and their implications for the Pacific–Indian throughflow and the global heat budget. *J. Geophys. Res.*, **98**, 6851–6868.
- Manabe, S., and R. J. Stouffer, 1988: Two stable equilibria of a coupled ocean–atmosphere model. *J. Climate*, **1**, 841–866.
- Mayer, D. A., and R. H. Weisberg, 1993: A description of COADS surface meteorological fields and the implied Sverdrup transports for the Atlantic Ocean from 30°S to 60°N. *J. Phys. Oceanogr.*, **23**, 2201–2221.
- McCartney, M. S., and L. D. Talley, 1984: Warm-to-cold water conversion in the northern North Atlantic Ocean. *J. Phys. Oceanogr.*, **14**, 922–935.
- , and R. A. Curry, 1993: Trans-equatorial flow of Antarctic Bottom Water in the western Atlantic Ocean: Abyssal geostrophy at the equator. *J. Phys. Oceanogr.*, **23**, 1264–1276.
- McClellan, J. L., and J. M. Klinck, 1995: Description and vorticity analysis of 50-day oscillations in the western tropical region of the CME model. *J. Phys. Oceanogr.*, **25**, 2498–2517.
- Mesinger, F., and A. Arakawa, 1976: Numerical methods used in atmospheric models. GARP Publ. Ser., Vol. 19, World Meteorological Organization, 64 pp.
- Metcalfe, W. G., 1968: Shallow currents along the northeastern coast of South America. *J. Mar. Res.*, **26**, 232–243.
- , and M. Stalcup, 1967: Origins of the Atlantic Equatorial Undercurrent. *J. Geophys. Res.*, **72**, 4959–4975.
- Metzger, E. J., H. E. Hurlburt, J. C. Kindle, Z. Sirkes, and J. M. Pringle, 1992: Hindcasting of wind driven anomalies using a reduced-gravity global ocean model. *Mar. Technol. Soc. J.*, **26** (2), 23–32.

- Mittelstaedt, E., 1989: The subsurface circulation along the Moroccan slope. *Poleward Flows Along Ocean Boundaries*, S. J. Neshyba, C. N. M. Mooers, R. L. Smith, and R. T. Barber, Eds., Springer-Verlag, 96–109.
- Molinari, R. L., and E. Johns, 1994: Upper layer temperature structure of the western tropical Atlantic. *J. Geophys. Res.*, **99**, 18 225–18 233.
- Munk, W. H., 1950: On the wind-driven ocean circulation. *J. Meteor.*, **7**, 79–93.
- Mysak, L. A., and G. J. Mertz, 1984: A 40- to 60-day oscillation in the source region of the Somali Current during 1976. *J. Geophys. Res.*, **89**, 711–715.
- NOAA, 1986: ETOP05 digital relief of the surface of the earth. Data Announce, 86-MGG-07, National Geophysical Data Center, Washington, D.C., 2 pp.
- Philander, S. G. H., and R. C. Pacanowski, 1986: The mass and heat budget in a model of the tropical Atlantic Ocean. *J. Geophys. Res.*, **91**, 14 192–14 206.
- Ponte, R. M., and D. S. Gutzler, 1992: 40–60 day oscillations in the western tropical Pacific: Results from an eddy-resolving global ocean model. *Geophys. Res. Lett.*, **19**, 1475–1478.
- Quadfasel, D. R., and J. C. Swallow, 1986: Evidence for 50-day period planetary waves in the South Equatorial Current of the Indian Ocean. *Deep-Sea Res.*, **33**, 1307–1312.
- Richardson, P. L., and D. Walsh, 1986: Mapping climatological seasonal variations of surface currents in the tropical Atlantic using shipdrifts. *J. Geophys. Res.*, **91**, 10 537–10 550.
- , G. E. Hufford, R. Limeburner, and W. S. Brown, 1994: North Brazil Current retroflection eddies. *J. Geophys. Res.*, **99**, 5081–5093.
- Rintoul, S. R., 1991: South Atlantic interbasin exchange. *J. Geophys. Res.*, **96**, 2675–2692.
- Roemmich, D., 1980: Estimation of meridional heat flux in the North Atlantic by inverse methods. *J. Phys. Oceanogr.*, **10**, 1972–1983.
- , 1983: The balance of geostrophic and Ekman transports in the tropical Atlantic Ocean. *J. Phys. Oceanogr.*, **13**, 1534–1539.
- Schmitz, W. J., Jr., 1996: On the interbasin-scale thermohaline circulation. *Rev. Geophys.*, **33**, 151–173.
- , and P. L. Richardson, 1991: On the sources of the Florida Current. *Deep-Sea Res.*, **38**, S389–S409.
- , and M. S. McCartney, 1993: On the North Atlantic circulation. *Rev. Geophys.*, **31**, 29–49.
- Schott, F. A., and C. W. Böning, 1991: The WOCE model in the western equatorial Atlantic: Upper layer circulation. *J. Geophys. Res.*, **96**, 6993–7004.
- , L. Stramma, and J. Fischer, 1995: The warm water inflow into the western tropical Atlantic boundary regime, spring 1994. *J. Geophys. Res.*, **100**, 24 745–24 760.
- Shriver, J. F., and H. E. Hurlburt, 1997: The contributions of the global thermohaline circulation to the Pacific to Indian through-flow via Indonesia. *J. Geophys. Res.*, **102**, 5491–5512.
- Stalcup, M. C., and W. G. Metcalf, 1972: Current measurements in the passages of the Lesser Antilles. *J. Geophys. Res.*, **77**, 1032–1049.
- Steger, J. M., and J. A. Carton, 1991: Long waves and eddies in the tropical Atlantic Ocean: 1984–1990. *J. Geophys. Res.*, **96**, 15 161–15 172.
- Stommel, H., 1960: *The Gulf Stream, A Physical and Dynamical Description*. University of California Press, 248 pp.
- Street-Perrott, F. A., and R. A. Perrott, 1990: Abrupt climate fluctuations in the tropics: The influence of Atlantic Ocean circulation. *Nature*, **343**, 607–612.
- Sverdrup, H. U., 1947: Wind-driven currents in a baroclinic ocean; with application to the equatorial currents of the eastern Pacific. *Proc. Natl. Acad. Sci.*, **33**, 318–326.
- , M. W. Johnson, and R. H. Fleming, 1942: *The Oceans, Their Physics, Chemistry, and General Biology*, Prentice-Hall, 1087 pp.
- Thompson, J. D., T. L. Townsend, A. Wallcraft, and W. J. Schmitz, 1992: Ocean prediction and the Atlantic basin: Scientific issues and technical challenges. *Oceanography*, **5**, 36–41.
- Wallcraft, A. J., 1991: The Navy Layered Ocean Model users guide. NOARL Rep. 35, Naval Research Laboratory, Stennis Space Center, MS, 21 pp. [Available from NRLSSC Classified Library, Stennis Space Center, MS 39529.]
- , and D. R. Moore, 1997: The NRL layered ocean model. *Parallel Compu.*, **23**, 2227–2242.
- Wilson, W. D., and W. E. Johns, 1997: Velocity structure and transport in the Windward Island Passages. *Deep-Sea Res.*, **44**(3), 487–520.
- , E. Johns, and R. L. Molinari, 1994: Upper layer circulation in the western tropical North Atlantic Ocean during August, 1989. *J. Geophys. Res.*, **99**, 22 513–22 523.
- Worthington, L. V., 1976: *On the North Atlantic Circulation*. The Johns Hopkins Oceanographic Studies, No. 6, The Johns Hopkins University Press, 110 pp.
- Wunsch, C., and B. Grant, 1982: Towards the general circulation of the North Atlantic Ocean. *Progress in Oceanography*, Vol. 11, Pergamon, 1–59.
- Youtsey, W. J. 1993: Report detailing modifications to the 1/8° global bathymetry. Naval Research Laboratory Rep. NRL/MR/7323-93-7023, Stennis Space Center, MS, 150 pp. [Available from NRLSSC Classified Library, Stennis Space Center, MS 39529.]